VIM-AS1 promotes proliferation and drives enzalutamide resistance in prostate cancer via IGF2BP2-mediated HMGCS1 mRNA stabilization

SHENG-JIA SHI[1-3*], DONG-HUI HAN[3*], JING-LIANG ZHANG[3*], YU LI[3], AN-GANG YANG[1] and RUI ZHANG[1]

[1]State Key Laboratory of Cancer Biology, Department of Immunology, Air Force Medical University, Xi'an, Shaanxi 710032; [2]Department of Andrology, Reproduction Center, Northwest Women's and Children's Hospital, Xian Jiaotong University Health Science Center, Xi'an, Shaanxi 710004; [3]Department of Urology, Xijing Hospital, Air Force Medical University, Xi'an, Shaanxi 710069, P.R. China

Received September 8, 2022; Accepted December 14, 2022

DOI: 10.3892/ijo.2023.5482

Abstract. VIM-AS1, a cancer-specific long non-coding RNA, has been recognized as a pivotal regulator in multiple types of cancer. However, the role of VIM-AS1 in the proliferation and resistance to anti-androgen therapy of LNCaP and C4-2 prostate cancer cells remains to be determined. In the current study, gain-and-loss experiments were used to investigate the effects of VIM-AS on the proliferation and anti-androgen therapy of LNCaP and C4-2 cells. RNA sequencing, RNA pulldown and RNA immunoprecipitation were used to elucidate the underlying mechanism of VIM-AS1 driving prostate progression. It was demonstrated that VIM-AS1 was upregulated in C4-2 cells, an established castration-resistant prostate cancer (CRPC) cell line, compared with in LNCaP cells, an established hormone-sensitive prostate cancer cell line. The present study further demonstrated that VIM-AS1 was positively associated with the clinical stage of prostate cancer. Functionally, overexpression of VIM-AS1 decreased the sensitivity to enzalutamide treatment and enhanced the proliferation of LNCaP cells *in vitro*, whereas knockdown of VIM-AS1 increased the sensitivity to enzalutamide treatment and reduced the proliferation of C4-2 cells *in vitro* and *in vivo*. Mechanistically, 3-hydroxy-3-methylglutaryl-CoA synthase 1 (HMGCS1) was identified as one of the direct downstream targets of VIM-AS1, and VIM-AS1 promoted HMGCS1 expression by enhancing HMGCS1 mRNA stability through a VIM-AS1/insulin like growth factor 2 mRNA binding protein 2 (IGF2BP2)/HMGCS1 RNA-protein complex. Rescue assays indicated that knockdown of HMGCS1 expression ameliorated the increase in proliferation and enzalutamide resistance of prostate cancer cells induced by VIM-AS1 overexpression. Overall, the present study determined the roles and mechanism of the VIM-AS1/IGF2BP2/HMGCS1 axis in regulating proliferation and enzalutamide sensitivity of prostate cancer cells and suggested that VIM-AS1 may serve as a novel therapeutic target for the treatment of patients with CRPC.

Correspondence to: Professor Rui Zhang or Professor An-Gang Yang, State Key Laboratory of Cancer Biology, Department of Immunology, Air Force Medical University, 169 Changle West Road, Xi'an, Shaanxi 710032, P.R. China
E-mail: ruizhang@fmmu.edu.cn
E-mail: agyang@fmmu.edu.cn

*Contributed equally

Abbreviations: lncRNA, long non-coding RNA; CRPC, castration-resistant prostate cancer; HSPC, hormone-sensitive prostate cancer; ADT, androgen deprival therapy; EMT, epithelial-mesenchymal transition; RT-qPCR, reverse transcription-quantitative PCR; GO, Gene Ontology; KEGG, Kyoto Encyclopedia of Genes and Genomes; GSEA, Gene Set Enrichment Analysis; RIP, RNA immunoprecipitation

Key words: VIM-AS1, 3-hydroxy-3-methylglutaryl-CoA synthase 1, insulin like growth factor 2 mRNA binding protein 2, enzalutamide resistance, mRNA stabilization

Introduction

Prostate cancer is a prevalent malignancy and has the highest incidence rate of all cancer types in men over the age of 65 years both in China and in the USA (1,2). During the initial stages of prostate cancer, androgen deprivation therapy (ADT) is the first line of treatment (3). Combined with radical prostatectomy or radiation therapy, ADT can effectively reduce the level of serum prostate specific antigen and suppress tumor growth (3). The majority of patients with hormone-sensitive prostate cancer (HSPC) who are initially sensitive to ADT gradually develop resistance to anti-androgen drugs such as enzalutamide or bicalutamide after 18-24 months of treatment (4). Consequently, HSPC progresses to castration-resistant prostate cancer (CRPC), which exhibits notably increased proliferation and metastasis (4). A previous study indicated that 90% of patients exhibit bone metastases when the CRPC further progresses to the metastatic CRPC stage, and those with distant metastasis exhibit poor 5-year survival rates of <3% (5). Therefore, there is an urgent need to determine the

detailed mechanisms underlying the development of ADT resistance and to identify novel therapeutic targets.

Numerous studies have confirmed that non-coding RNAs serve important roles in the carcinogenesis and progression of several types of cancer (6,7). Long non-coding RNAs (lncRNAs) are a novel class of endogenous non-coding RNAs, which are pervasively transcribed from the human genome and are >200 nucleotides in length (8). Previously, lncRNAs were considered to be the byproducts of RNA splicing errors with no or limited physiological and pathological functions (9). With the rapid development of high-throughput sequencing technologies, an increasing number of lncRNAs have been found and identified as key regulators of biological and/or pathological behaviors during the occurrence and progression of numerous diseases, including prostate cancer, glioma, gastric cancer and cholangiocarcinoma (7,9-11). For example, it has been reported that lncRNA 01614 promoted pancreatic cancer progression by suppressing GSK-3β (12). Zhang *et al* (13) reported that LncKRT16P6 promoted tongue squamous cell carcinoma progression by functioning as a competing endogenous RNA. In prostate cancer, the majority of previous studies have paid attention to the effects of lncRNAs on the proliferation and metastasis of cancer cells (10,14,15), while the expression patterns and functions of lncRNAs in the progression from HSPC to CRPC remain overlooked.

A previous study demonstrated that there were 134 differentially expressed lncRNAs between LNCaP (an established androgen-dependent prostate cancer cell line typically used as an *in vitro* model for HSPC) and C4-2 cells (an established androgen-independent prostate cancer cell line typically used as an *in vitro* model for CRPC) using high-throughput lncRNA sequencing (16). This suggested that these lncRNAs may be involved in the process of ADT resistance. Furthermore, the expression profiles of the four most upregulated lncRNAs (plncRNA-1, Linc00963, SNHG17 and VIM-AS1) were confirmed in LNCaP and C4-2 cells to verify the lncRNA sequencing results. The follow-up studies successively identified that these four lncRNAs accelerated progression by sponging microRNAs (miRNAs/miRs) or mediating epithelial-mesenchymal transition (EMT) (17-19). However, the specific mechanisms by which VIM-AS1 increased proliferation and promoted the acquisition of enzalutamide resistance in prostate cancer requires further elucidation.

In the present study, it was demonstrated that VIM-AS1 was highly expressed in CRPC and this was indicative of poor disease-free survival. It was also revealed that VIM-AS1 promoted proliferation and induced enzalutamide resistance *in vitro* and *in vivo*. Notably, VIM-AS1 was demonstrated to interact with insulin like growth factor 2 mRNA binding protein 2 (IGF2BP2) protein to enhance the mRNA stability of 3-hydroxy-3-methylglutaryl-CoA synthase 1 (HMGCS1), which further resulted in malignant proliferation and enzalutamide resistance.

Materials and methods

Cell culture. LNCaP (cat. no. TCHu73), VCaP (cat. no. TCHu220) and PC-3 (cat. no. TCHu158) human prostate cancer cell lines were obtained from The Cell Bank of Type Culture Collection of The Chinese Academy of Sciences. DU145 (cat. no. HTB-81) human prostate cancer cells were obtained from American Type Culture Collection. C4-2 (cat. no. CL-0046) human prostate cancer cells were obtained from Procell Life Science & Technology Co., Ltd. LNCaP, VCaP, C4-2 and DU145 cells were maintained in DMEM (HyClone; Cytiva) supplemented with 10% FBS (Cellmax) and 1% penicillin-streptomycin (Gibco; Thermo Fisher Scientific, Inc.). PC-3 cells were cultured with DMEM/F12 (HyClone; Cytiva) with 10% FBS (Cellmax) and 1% penicillin-streptomycin (Gibco; Thermo Fisher Scientific, Inc.). All cells were kept in a humidified incubator supplied with 5% CO_2 at 37˚C.

Transfection. VIM-AS1 overexpression vector (VIM-AS1 OE; cat.no.PG1-21050014; plasmid backbone, pcDNA3.1), IGF2BP2 overexpression vector (IGF2BP2 OE; cat. PB1-20100010; plasmid backbone, pcDNA3.1) and HMGCS1 overexpression vector (HMGCS1 OE; cat. no. PB1-20100011; plasmid backbone, pcDNA3.1), and pcDNA3.1 empty vector (Vector; cat. no. CL-0046) were purchased from Genecreate. VIM-AS1 short hairpin RNA (shRNA/sh) (sh-VIM-AS1; target sequence, 5'-GCTCCCTTTGGATGACATAGA-3'; plasmid backbone, GV344) and normal scramble short hairpin RNA (sh-NC; control sequence, 5'-TTCTCCGAACGTGTCACGT-3'; plasmid backbone, GV344) were purchased from Shanghai GeneChem Co., Ltd. IGF2BP2 small interfering RNA (si-IGF2BP2), HMGCS1 small interfering RNA (si-HMGCS1) and non-targeting control small interfering RNA (siRNA/si) (si-NC; sequence) were purchased from Guangzhou RiboBio Co., Ltd and the sequences of siRNAs are listed in Table SI. The vector and siRNA transfections were performed as described previously (20). Briefly, ~1x10^6 prostate cancer cells, which were seeded in six-well plates, were transfected with 0.5 μg vector or siRNAs using 2.5 μl Lipofectamine® 2000 (Thermo Fisher Scientific, Inc.) at 37˚C for 48 h according to the manufacturer's protocol. Cells were collected for reverse transcription-quantitative PCR (RT-qPCR), western blotting, Cell Counting Kit-8 (CCK-8) assays, 5-ethynyl-2'-deoxyuridine (EdU) assays, colony formation assays, chemosensitivity assays, TUNEL assays and flow cytometry analysis 48 h after siRNA transfection. shRNA infections were performed as described previously (21). sh-VIM-AS1 (lentiviral plasmid, GV344; GeneChem, Inc.) and sh-NC were packaged in 293T cells (cat. no. CRL-3216; American Type Culture Collection) using a 2nd generation system with the ratio of lentiviral construct, packaging plasmid (Helper 1.0; GeneChem, Inc.) and envelope plasmid (Helper 2.0; GeneChem, Inc.) (20 μg:15 μg:10 μg). The culture medium was centrifugated at 1,000 x g for 5 min at 4˚C after 293T cells were cultured for 48 h at 37˚C. The supernatant containing viral particles was collected. After C4-2 cells were infected with sh-VIM-AS1 and sh-NC (multiplicity of infection, 50) at 37˚C for 48 h, the efficiency was initially validated by assessing VIM-AS1 expression using RT-qPCR. The cells were then selected using puromycin at a concentration of 2 μg/ml for 2 weeks to obtain C4-2 cells with stable knockdown of VIM-AS1. Subsequently, the cells were maintained in complete medium with puromycin at a concentration of 0.5 μg/ml and collected for RT-qPCR, western blotting, CCK-8 assays, EdU assays, colony formation assays, chemosensitivity assays, TUNEL assays and flow cytometry analysis 48 h after shRNA infection.

RNA extraction and RT-qPCR. A Cytoplasmic & Nuclear RNA Purification Kit (Norgen Biotek Corp.) was used to isolate cytoplasmic and nuclear RNA of C4-2 cells according to the manufacturer's protocol. Total RNA from prostate cancer cells and resected tumor tissues was isolated using TRIzol® solution (Invitrogen; Thermo Fisher Scientific, Inc.). For VIM-AS1, HMGCS1 mRNA and IGF2BP2 mRNA expression analysis, the aforementioned RNA extracts were reverse transcribed using a RevertAid First Strand cDNA Synthesis Kit (Beijing Solarbio Science & Technology Co., Ltd.) according to the manufacturer's protocol, followed by amplification and quantification using a 2x SYBR Green PCR MasterMix Kit (Beijing Solarbio Science & Technology Co., Ltd.) according to the manufacturer's protocol. CFX96 real time PCR detection system (Bio-Rad Laboratories, Inc.) was used for quantitative detection with the following thermocycling conditions: Initial denaturation at 95˚C for 2 min, followed by 25 cycles of denaturation at 95˚C for 15 sec, annealing at 60˚C for 30 sec and extension at 72˚C for 1 min. The relative expression levels were determined using the $2^{-\Delta\Delta Cq}$ method (22). GAPDH was used as the internal control. The primers used in the present study were purchased from Sangon Biotech Co., Ltd. and are shown in Table SI.

Protein extraction and western blotting. Total protein from prostate cancer cells was extracted using RIPA lysis buffer (cat. no. G2002; Wuhan Servicebio Technology Co., Ltd.) supplemented with protease inhibitors (Beijing Solarbio Science & Technology Co., Ltd.). After determining the concertation of each proteins using a BCA protein assay kit (cat. no. G2026; Wuhan Servicebio Technology Co., Ltd.), a total of 30 μg protein per lane was loaded on a 10% SDS-gel, resolved using SDS-PAGE and transferred to a PVDF membrane. The membranes were blocked with 5% nonfat dry milk at room temperature for 2 h, and then incubated with anti-HMGCS1 (cat. no. ab155787; 1:500; Abcam), anti-IGF2BP2 (cat. no. ab117809; 1:500; Abcam) or anti-GAPDH (cat. no. ab9485; 1:500; Abcam) primary antibodies overnight at 4˚C, and subsequently incubated with an HRP-labeled goat-anti-rabbit (cat. no. 7074; 1:5,000; Cell Signaling Technology, Inc.) secondary antibody for 2 h at room temperature. The bands were visualized using Immobilon™ Western Chemilum HRP Substrate (cat. no. WBKLS0100, MilliporeSigma) and analyzed using Quantity One software version 4.6.6 (Bio-Rad Laboratories, Inc.).

Chemosensitivity assay. A total of $3x10^3$ cells/well were plated into a 96-well plate. After adherence, cells were treated with different concentrations (0, 1, 1.5, 2, 2.5, 3, 3.5, 4, 5, 10, 20, 30, 40, 50 μM) of enzalutamide at 37˚C for 72 h. Subsequently, 10 μl/well CCK-8 solution (cat. no. K1018; Dojindo Molecular Technologies, Inc.) was added to the culture medium. The cells were incubated with CCK-8 reagent at 37˚C for 1 h and the optical density values at 450 nm were measured using a microplate reader. The IC_{50} value was calculated as previously described (23).

Colony formation assay. A total of 500 C4-2 cells infected with sh-NC and sh-VIM-AS1 and LNCaP cells transfected with Vector and VIM-AS1 OE per well were plated into a 6-well plate. After 10 days of incubation at 37˚C, the colonies were washed with PBS, fixed with 90% methanol at room temperature for 10 min and stained with crystal violet for 15 min at room temperature. Subsequently, the colonies (>50 cells) were imaged using a digital camera (version D3200; Nikon Corporation) at x4 magnification and quantified using Image J software (version 1.5; National Institutes of Health).

TUNEL assay. TUNEL assays were performed using an *In Situ* Cell Death Detection Kit (cat. no. 11684817910; Roche Diagnostics GmbH) according to the manufacturer's instructions. Briefly, $1x10^5$ cells/well were seeded in 96-well plates and cultured with complete medium for 48 h at 37˚C. Subsequently, cells were stained with 50 μl terminal deoxynucleotidyl transferase for 1 h in the dark at 37˚C and 450 μl fluorescein-labeled deoxyuridine triphosphate solution for 1 h in the dark at 37˚C after cell fixation by 4% paraformaldehyde for 30 min at room temperature and permeabilization by 0.5% TRITON X-100 for 90 sec at 4˚C. Next, cells were stained with TUNEL reaction mixture and DAPI-containing mounting media (0.5 mg/ml; cat. no. S2110; Beijing Solarbio Science & Technology Co., Ltd.) for 1 h in the dark at 37˚C. Three visual fields were randomly selected for observation using a laser scanning confocal microscope (FV1000; Olympus Corporation) and corresponding software (FV10-ASW Viewer; version 4.2; Olympus Corporation) at x200 magnification.

EdU staining. EdU assays were conducted using a Cell-Light™ EdU DNA Cell Proliferation Kit (cat. no. C10310-1; Guangzhou RiboBio Co., Ltd.) according to the manufacturer's instructions. Briefly, $1x10^5$ cells/well were seeded in 96-well plates and cultured with complete medium for 48 h at 37˚C. Cells were stained with 100 μl 50 μM EdU solution for 2 h in the dark at room temperature. The cells were stained with Apollo®567 (Guangzhou RiboBio Co., Ltd.) for 30 min at 4˚C and DAPI for 10 min at 4˚C after cell fixation by 4% paraformaldehyde for 30 min at room temperature and permeabilization by 0.5% TRITON X-100 for 90 sec at 4˚C. Three visual fields were randomly selected for observation using a laser scanning confocal microscope (FV1000; Olympus Corporation) and corresponding software (FV10-ASW Viewer; version 4.2; Olympus Corporation) at x200 magnification.

Flow cytometry assay. Cell apoptosis and cell cycle analyses were performed using an Annexin V Alexa fluor 488/PI Cell Apoptosis Kit and DNA Content Quantitation Kit (cat. no. CA1040; Beijing Solarbio Science & Technology Co., Ltd.) according to the manufacturer's instructions. Briefly, $1x10^6$ cells/well were seeded in 6-well plates and cultured for 48 h at 37˚C. For cell apoptosis, $1x10^6$ cells were harvested and stained with annexin-V and PI for 30 min at 4˚C. For cell cycle analysis, $1x10^6$ cells were harvested and stained with PI for 30 min at 4˚C after fixing with 70% ethanol for 30 min at 4˚C. Early cell apoptosis (lower right quadrant-prophase apoptosis; Beijing Solarbio Science & Technology Co., Ltd.) and cell cycle (Beijing Solarbio Science & Technology Co., Ltd.) distribution analyses were performed using a flow cytometer (CytoFLEX LX; Beckman Coulter, Inc.). All data were analyzed with Flowjo version 10.0.6 (Becton, Dickinson and Company).

High-throughput sequencing analysis. Total RNA was isolated from transfected LNCaP cells. Subsequently, 1.3 μg total RNA was sent for RNA sequencing (RNA-seq; Genecreate Co., Ltd.). RNA libraries for RNA-seq were prepared using a NEBNext® Ultra™ RNA Library Prep Kit for Illumina® (cat. no. NEB+e7770; New England BioLabs, Inc.) according to the manufacturer's protocols (New England BioLabs, Inc.). The loading concentration of the constructed library was detected using the Agilent High Sensitivity DNA kit (cat. no. 5067-4626; Agilent Technologies, Inc.) and an Agilent 2100 bioanalyzer (Agilent Technologies, Inc), and was 6 pM for RNA-seq. Libraries which consisted of cDNA fragments of 200 bp in length were sequenced on the Illumina NovaSeq 6000 (150 base pairs; paired ends; Illumina, Inc.) using a MiniSeq High Output Reagent Kit (cat. no. FC-420-1002; Illumina, Inc.). Sequence reads were trimmed for adaptor sequence/low-quality sequence using fastp (version 0.12.0; https://github.com/OpenGene/fastp) (24). Trimmed sequence reads were mapped to hg38 using Hisat2 software (version 2.2.1; http://daehwankimlab.github.io/hisat2/) (25). Reads per kilo-base of exon per megabase of library size were calculated using featureCounts (version 1.5.3; http://bioinf.wehi.edu.au/featureCounts/) (26). Differentially expressed genes were identified according to |log2(fold change)|>1 and P<0.05 using the R program (version 4.03; http://www.r-project.org). Next, Gene Ontology (GO; http://geneontology.org/) (27,28) analysis, Kyoto Encyclopedia of Genes and Genomes (KEGG; https://www.kegg.jp/) (29) analysis, and Gene Set Enrichment Analysis (GSEA; http://www.gsea-msigdb.org/gsea/index.jsp) were used to further analyze the differentially expressed genes. The significance cult-off level was P<0.05.

RNA pull-down. Cells were lysed in NP40 lysis buffer (cat. no. N8030; Beijing Solarbio Science & Technology Co., Ltd.), and 1 mg cell extracts were incubated with a biotin-labeled VIM-AS1 (Genecreate Co., Ltd.; sequence, 5'-UCCCUGAGAUGAUGAAGAGGACCAGUGCCCAUUCCAGGA-3') or a normal scrambled control (NC; Genecreate Co., Ltd.; sequence, 5'-UAUCACGUAGCCGUUGCAUUUGCCGUAGCCCUGUGGGCC-3') probe at 4˚C for 6 h. Subsequently, cell extracts, biotin-labeled VIM-AS1 or NC, and 40 μl streptavidin agarose beads were mixed and incubated on a rotator overnight at 4˚C. After washing with PBS, precipitates were pulled down by centrifugation at 3,000 x g for 5 min at 4˚C. The potential binding proteins in the retrieved precipitates were identified by high performance liquid chromatography-mass spectrometry (HPLC-MS) detection (Genecreate Co., Ltd.). HPLC-MS analysis was performed on a Orbitrap Exploris 480-mass spectrometer (Thermo Fisher Scientific, Inc.) that was coupled to a Nanospray Flex™ (Thermo Fisher Scientific, Inc.) for 60 min. The mass spectrometer was operated in positive ion mode to monitor the m/z transitions for all peptides. Target peptides (two for each protein) were measured in multiple reaction monitoring (MRM). Peptide ions between 350 and 1,200 m/z were scanned in the Orbitrap detector (Thermo Fisher Scientific, Inc.) every 3 sec with a resolution of $1.2x10^5$ (maximum fill time 50 msec; automatic gain control target $4x10^5$). A scheduled MRM acquisition method was constructed using manually optimized decluttering potentials, collision energies, collision cell entrance and exit potentials.

mRNA stability assay. A total of $1x10^6$ cells were seeded in 6-well plates and cultured overnight. The following day, 5 μg/ml actinomycin D (cat. no. HY-17559; MedChemExpress) was added to cells to inhibit gene transcription for 2, 4, 6 or 8 h at 4˚C. At the indicated times, the mRNA levels of HMGCS1 were determined using RT-qPCR as aforementioned.

RNA immunoprecipitation (RIP). RIP assays were performed using a Magna RIP™ RNA-Binding Protein Immunoprecipitation Kit (cat. no. 17-704; MilliporeSigma) according to the manufacturer's instructions. Briefly, a total of $1x10^7$ cells were collected, centrifuged at 4˚C for 5 min at 1,000 x g, washed in pre-cooled PBS, and then lysed using complete RIP Lysis buffer (cat. no. R0010; Beijing Solarbio Science & Technology Co., Ltd.). A total of 5 μg anti-IGF2BP2 (cat. no. ab117809; 1:500; Abcam) or lgG (cat. no. ab172730; 1:500; Abcam) was added to 50 μl protein A/G magnetic bead suspension for 30 min at room temperature. Subsequently, 100 μl of the aforementioned lysates were incubated with the beads-antibody complex overnight at 4˚C. After washing with RIP wash buffer (part of the Magna RIP™ RNA-Binding Protein Immunoprecipitation Kit) three times, Protease K buffer (cat. no. P1120; Beijing Solarbio Science & Technology Co., Ltd.) was added to the immunoprecipitated product, followed by incubation at 55˚C for 30 min. Following centrifugation at 4˚C for 5 min at 1,000 x g, the immunoprecipitated RNA was isolated using TRIzol® reagent (Invitrogen; Thermo Fisher Scientific, Inc.) and analyzed using RT-qPCR as aforementioned.

Fluorescence in situ hybridization (FISH). FISH assays were performed using a RiboTM lncRNA FISH probe Mix Kit (cat. no. c10910; Guangzhou RiboBio Co., Ltd.) according to the manufacturer's instructions. Oligonucleotide modified Cy-3-labeled probes for VIM-AS1 (5'-TAGGACTTCCTAGTACTTCTGA-3), GAPDH and U6 were designed and synthesized by Genecreate. C4-2 cells were seeded on 20-mm confocal dishes (Corning, Inc). After overnight incubation, C4-2 cells were fixed with 4% paraformaldehyde for 20 min at 4˚C and permeabilized using Triton X-100 for 90 sec at 4˚C. Next, 250 μl prehybridization solution with 1% blocking solution (Guangzhou RiboBio Co., Ltd.) was added to C4-2 cells and cells were incubated at 42˚C for 1 h. Subsequently, C4-2 cells were incubated with 100 μl hybridization buffer (Guangzhou RiboBio Co., Ltd.) supplemented with 1% blocking solution and 2.5 μl 20 μM 22-nucleotide CY-3-labeled-VIM-AS1, CY-3-labeled-GAPDH or CY-3-labeled-U6 FISH probe at 37˚C overnight in a dark moist chamber. The following day, cells were washed three times in 2X sodium citrate buffer for 5 min at 42˚C and stained with DAPI at 4˚C for 10 min. Images were acquired using a laser scanning confocal microscope (FV1000; Olympus Corporation) and corresponding software (FV10-ASW Viewer; version 4.2; Olympus Corporation) at a magnification of x400.

In vivo experiments. All animal experiments were performed in accordance with the relevant national ethical regulations and were approved by the Animal Care and Use Committee of the Air Force Medical University (approval no: 20220967; Xi'an, China). All mice were purchased from Beijing Vital

River Laboratory Animal Technology Co., Ltd., and housed in an animal room at a controlled temperature of 22˚C and 40% humidity, with a 12 h light/dark cycle, and *ad libitum* access to food and water. Female BALB/c nude mice (6 weeks old; n=12; weight, ~20 g) were used to establish the C4-2 xenograft models. 100 μl C4-2 cells (5x10^6/100 μl PBS) infected with sh-VIM-AS1 or sh-NC were injected subcutaneously into the left upper limb of the nude mice. For the following 5 weeks, the health and behavior of the mice were monitored twice a week, and tumor growth was monitored using a vernier caliper twice a week and an *in vivo* imaging system once a week. When the humane endpoints were reached or the tumor volume of mice in the sh-VIM-AS1 or sh-NC groups was closed 1,000 mm^3, the mice would be euthanized. According to the requirements of the Animal Center of Air Force Medical University (Xi'an, China), humane endpoints were reached when the xenograft tumor diameter was >20 mm, or signs of unrelieved pain or distress without recovery were observed. At the end of 35 days of observation, all 12 mice had not reached human endpoints but the largest tumor volume was 892.4 mm^3. Therefore, all 12 mice were sacrificed by acute exsanguination following isoflurane inhalation (5% for induction and 2% for maintenance of 5 min), cardiac arrest was then used to verify death based on a lack of a heartbeat. The tumors were excised and assessed using immunohistochemistry and RT-qPCR, and the tumor volumes and weights were measured.

Immunohistochemistry. Resected tumor tissues were fixed with 4% paraformaldehyde at 4˚C for 24 h. The tissues were embedded in paraffin and sectioned (4 μm). After conventional dewaxing and rehydration with descending alcohol series at room temperature, the sections were incubated with 3% H_2O_2 for 15 min. The sections were incubated with 5% normal goat serum (SL038; Beijing Solarbio Science & Technology Co., Ltd.) at room temperature for 1 h. Subsequently, Ki-67 antibody (cat. no. GB121141; 1:1,000; Wuhan Servicebio Technology Co., Ltd.) or HMGCS1 antibody (cat. no. ab155787; 1:500; Abcam) were added for incubation at 4˚C overnight after antigen retrieval with citric acid buffer (pH 6.0) for 1 min 40 sec at 100˚C in a pressure cooker. Subsequently, the sections were incubated with HRP-conjugated secondary antibody (cat. no. G1214; 1:200; Wuhan Servicebio Technology Co., Ltd.) at room temperature for 1 h. The sections were rinsed three times using TBS with 0.1% Tween-20 for 5 min and visualized using DAB solution (cat. no. G1212; 1:1,000; Wuhan Servicebio Technology Co., Ltd.) for 10 min at room temperature. Images were acquired using a light microscope at a magnification of x200.

Bioinformatics analysis. RNA-seq expression profiles and corresponding clinical information for VIM-AS1 in prostate cancer were downloaded from The Cancer Genome Atlas (TCGA; https://portal.gdc.cancer.gov/projects/TCGA-PRAD; project ID, TCGA-PRAD, mRNA sequencing data) and the Gene Expression Omnibus (GEO) database (dataset no. 32269, https://www.ncbi.nlm.nih.gov/geo/query/acc.cgi?acc=GSE32269) (30) and analyzed using the R program (version 4.03; http://www.r-project.org). The m6A modification status was predicted using Whistle (http://180.208.58.19/whistle/index.html). The gene (HMGCS1) was entered in the search box. m6A predicted modification sites were listed. P<0.05 was considered to indicate a statistically significant difference.

Statistical analysis. GraphPad Prism version 8.02 (GraphPad Software; Dotmatics) and SPSS version 22.0 (IBM Corp.) were used to perform statistical analysis. Data are presented as the mean ± SD or as scatter dot plots. All experiments were repeated three times. Unpaired Student's t-test was used to compare the difference between two groups, and one-way ANOVA followed by post hoc tests (least significant difference test for three groups and Bonferroni test for more than three groups) was used for comparisons among multiple groups. A Kruskal-Wallis test followed by a Bonferroni test was used to compare the difference of VIM-AS1 expression in patients with prostate cancer with different T stage and normal controls. Kaplan-Meier survival curves and the log-rank test were used to compare the differences in disease-free survival of patients with prostate cancer with different VIM-AS1 expression in TCGA dataset (project ID, TCGA-PRAD; mRNA data; cutoff-high, 75%; cutoff-low, 25%). The following parameters were selected: Disease-free survival, split patients by lower quartile, follow-up threshold: 14 years. Log rank P-values <0.05 for the Kaplan-Meier plots of patients with prostate cancer with different VIM-AS1 expression were considered to indicate a statistically significant difference. P-values were determined using a two-sided test. P<0.05 was considered to indicate a statistically significant difference.

Results

VIM-AS1 expression is upregulated in patients with advanced prostate cancer, and C4-2, PC-3 and DU145 cells. A previous study indicated that VIM-AS1 was upregulated in C4-2 cells compared with LNCaP cells (14). To further assess the differential expression profiles of VIM-AS1 during the progression of prostate cancer, VIM-AS1 expression was analyzed using TCGA and GEO (GSE32269). VIM-AS1 expression was consistently increased in advanced prostate cancer based on the data from TCGA (P<0.001; Fig. 1A). In addition, VIM-AS1 was upregulated in the tissues of patients with CRPC compared with those of patients in the HSPC group based on the GSE32269 dataset from GEO (P<0.001; Fig. 1B). Furthermore, Kaplan-Meier survival data indicated that patients with prostate cancer with high VIM-AS1 expression exhibited worse disease-free survival compared with patients with low VIM-AS1 expression (P=0.003; Fig. 1C). Increased VIM-AS1 expression was also observed in androgen-independent prostate cancer cell lines (DU145, PC-3 and C4-2) compared with LNCaP and VCaP cell lines, which are androgen-dependent prostate cancer cell lines (Fig. 1D). These data indicated that VIM-AS1 expression was upregulated in advanced prostate cancer.

VIM-AS1 enhances proliferation and induces enzalutamide resistance in prostate cancer cells in vitro. To examine the effects of VIM-AS1, VIM-AS1 was stably overexpressed in LNCaP cells and VIM-AS1 expression was knocked down in C4-2 cells. RT-qPCR demonstrated that transfection with the VIM-AS1 overexpression vector increased VIM-AS1

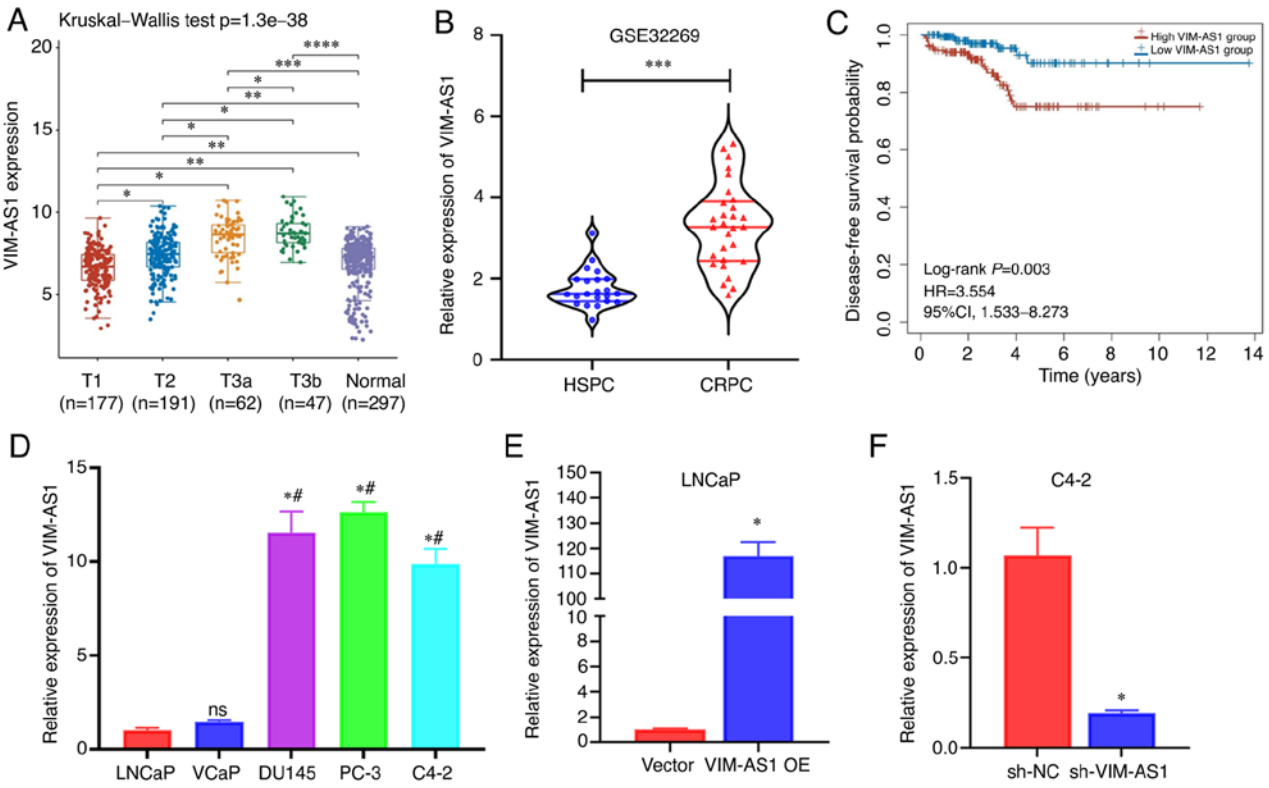

Figure 1. VIM-AS1 expression is associated with tumor stage and androgen deprivation therapy resistance. (A) TCGA data of VIM-AS1 expression in patients with prostate cancer with different T stages. (B) Gene Expression Omnibus data of VIM-AS1 expression in patients with CRPC and HSPC. (C) Kaplan-Meier survival curves of disease-free survival probability in patients with prostate cancer based on data obtained from TCGA. Patients were stratified into low and high VIM-AS1 expression group. (D) VIM-AS1 expression in two HSPC cell lines (LNCaP and VCaP) and three CRPC cell lines (DU145, PC-3 and C4-2). (E) VIM-AS1 levels in LNCaP cells transfected with VIM-AS1 OE or vector. (F) Detection of VIM-AS1 levels in C4-2 cells transfected with sh-VIM-AS1 or sh-NC. *P<0.05 vs. LNCaP or as indicated, $^{\#}$P<0.05 vs. VCaP, ^{ns}P>0.05 vs. LNCaP, **P<0.01, ***P<0.001, ****P<0.0001. CRPC, castration-resistant prostate cancer; HR, hazard ratio; HSPC, hormone-sensitive prostate cancer; ns, not significant; sh-NC, normal scramble short hairpin RNA; TCGA, The Cancer Genome Atlas.

expression in LNCaP cells (P<0.05; Fig. 1E), whereas sh-VIM-AS1 transfection stably knocked down VIM-AS1 expression in C4-2 cells (P<0.05; Fig. 1F). Furthermore, it was demonstrated that the IC_{50} of enzalutamide was increased after overexpression of VIM-AS1 in LNCaP cells (P<0.05; Figs. 2A and S1A). However, the IC_{50} of enzalutamide was decreased after the knockdown of VIM-AS1 in C4-2 cells (P<0.05; Figs. 3A and S1A). Colony formation and EdU assays indicated that the proliferation of VIM-AS1-overexpressing LNCaP cells was significantly increased compared with that of the control group (P<0.05; Figs. 2B and C, and S1B and C), and sh-VIM-AS1-infected C4-2 cells exhibited significantly reduced proliferation compared with the sh-NC-infected cells (P<0.05; Figs. 3B and C, and S1B and C). In addition, TUNEL and flow cytometry analyses demonstrated that overexpression of VIM-AS1 significantly reduced apoptosis, increased the percentage of cells in the S stage, and decreased the percentage of cells in the G1 stage in LNCaP cells (P<0.05; Figs. 2D-F and S1D-F), whereas cell apoptosis and the percentage of cells in the G1 stage were markedly enhanced and the percentage of cells in the S stage was decreased following VIM-AS1 knockdown in C4-2 cells (P<0.05; Figs. 3D-F and S1D-F). Collectively, these data suggested that aberrant upregulation of VIM-AS1 served an important role in promoting proliferation and driving enzalutamide resistance in prostate cancer *in vitro*.

Effects of VIM-AS1 on tumor growth in a prostate cancer xenograft model. A nude mouse model was used to validate the effects of knockdown of VIM-AS1 on the proliferation of prostate cancer cells *in vivo*. C4-2 cells with stable knockdown of VIM-AS1 were injected into nude mice via subcutaneous injection. Small animal *in vivo* imaging and growth curves indicated that the mice injected with the VIM-AS1 knockdown C4-2 cells exhibited slower tumor growth than the mice in the sh-NC group (Fig. 4A and B). Similarly, the sizes and weights of the dissected tumors from nude mice indicated that knockdown of VIM-AS1 suppressed tumor growth of prostate cancer cells *in vivo* (Fig. 4C and D). VIM-AS1 expression was lower in the resected tissues from the sh-VIM-AS1 group compared with the sh-NC group (Fig. S2A). Ki-67 and TUNEL assays indicated that the subcutaneous tumors in the VIM-AS1 knockdown group had fewer Ki-67-positive cells (P<0.05; Fig. 4E) and more TUNEL-positive cells (P<0.05; Fig. 4F) compared with those in the sh-NC group. Overall, these results indicated that knockdown of VIM-AS1 expression in C4-2 cells markedly suppressed tumor growth of prostate cancer *in vivo*.

HMGCS1 is involved in the functions of VIM-AS1 in prostate cancer cells. Next, it was attempted to determine the mechanism through which VIM-AS1 regulated the proliferation and enzalutamide sensitivity of prostate cancer

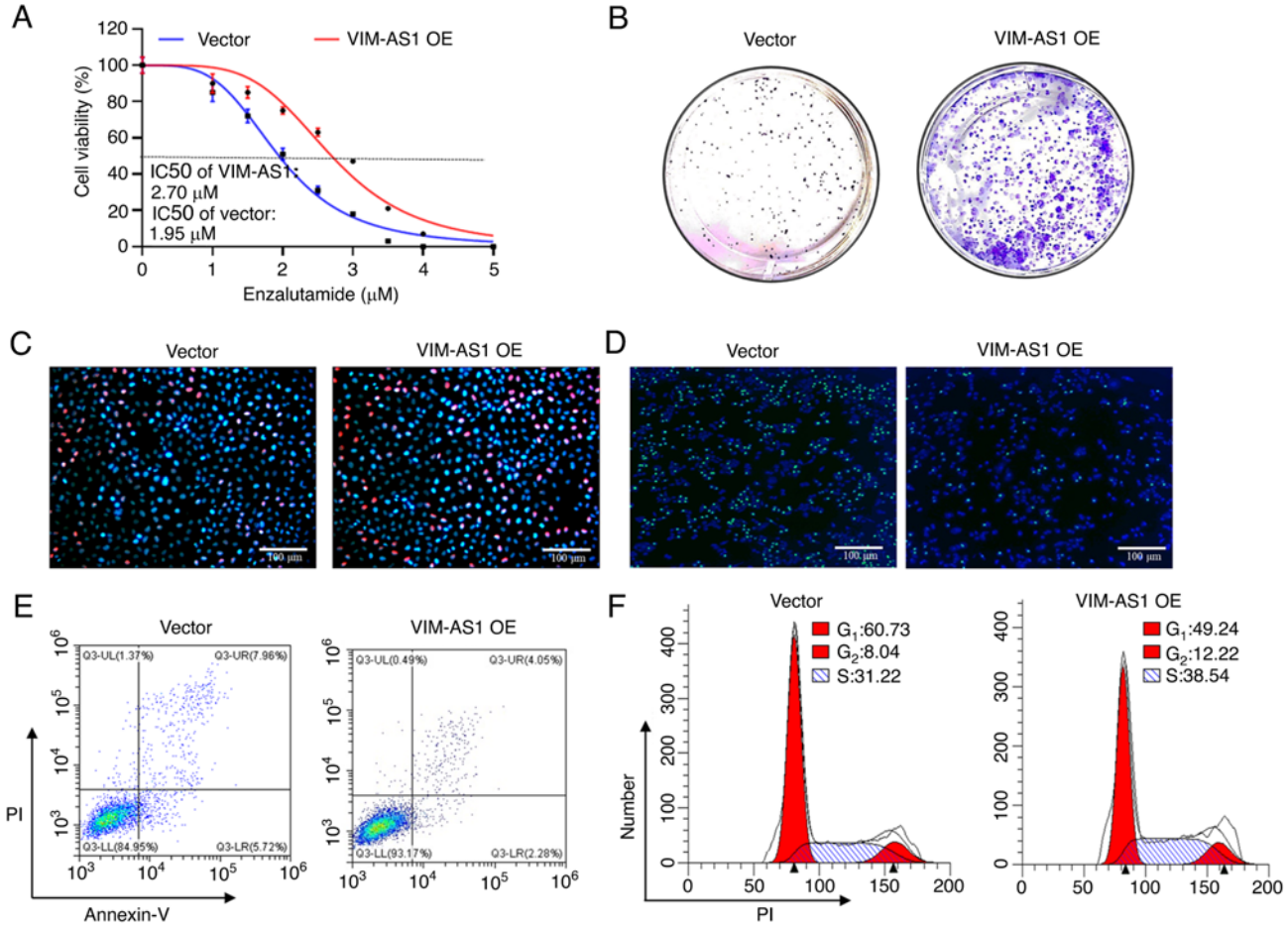

Figure 2. Effects of VIM-AS1 overexpression on enzalutamide sensitivity and proliferation in LNCaP cells. (A) Effect of VIM-AS1 overexpression on the viability of LNCaP cells treated with different concentrations of enzalutamide for 72 h as detected using a Cell Counting Kit-8 assay. (B) Effects of VIM-AS1 overexpression on the colony formation of LNCaP cells. (C) Effects of VIM-AS1 overexpression on the proliferation of LNCaP cells as detected using a 5-ethynyl-2'-deoxyuridine assay. Scale bar, 100 μm. (D) Effects of VIM-AS1 overexpression on the apoptosis of LNCaP cells as detected using TUNEL assays. Scale bar, 100 μm. (E) Effects of VIM-AS1 overexpression on the apoptosis of LNCaP cells as assessed using flow cytometry. (F) Effects of VIM-AS1 overexpression on cell cycle distribution of LNCaP cells as detected using flow cytometry.

cells. First, RNA-seq was used to identify the target genes in VIM-AS1-overexpressing LNCaP cells and vector-transfected cells. A total of 67 genes were found to be statistically upregulated by |log2(fold change)|>1 and 187 genes were found to be statistically downregulated by |log2(fold change)|>1 in VIM-AS1-overexpressing LNCaP cells (Fig. 5A). Notably, HMGCS1 was one of the most significantly upregulated genes in VIM-AS1-overexpressing cells (Fig. 5B). KEGG analysis showed that Steroid biosynthesis, Fat digestion and absorption and HIF-1 signaling pathway etc. were among the top 20 most enriched pathways (Fig. 5C). GO analysis demonstrated the 'steroid biosynthetic process', 'unfolded protein binding' and 'double-stranded RNA binding' were among the top 20 most enriched functions (Fig. 5D). Furthermore, GSEA demonstrated that the gene signatures of 'Steroid biosynthesis' were enriched in VIM-AS1-overexpressing cells (Fig. 5E). Notably, a previous study has reported that HMGCS1 was actively involved in steroid biosynthesis (31). As indicated by IHC analyses (Fig. S2B), RT-qPCR (Figs. 5F and S2C), and western blotting (Fig. 5G), the mRNA and protein levels of HMGCS1 were upregulated in LNCaP cells transfected with the VIM-AS1 overexpression vector *in vitro* (Fig. 5F and G), but downregulated in C4-2 cells transfected with sh-VIM-AS1 compared with the vector-transfected cells *in vitro* (Fig. 5F and G) and *in vivo* (Fig. S2B and C) (all P<0.05). Next, it was assessed whether VIM-AS1 regulated HMGCS1 expression by stabilizing HMGCS1 mRNA. To test this hypothesis, prostate cancer cells were treated with actinomycin D to measure the degradation of HMGCS1 mRNA. VIM-AS1 overexpression enhanced HMGCS1 mRNA stability, and VIM-AS1 knockdown significantly reduced HMGCS1 mRNA stability (at 4, 6 and 8 h; P<0.05; Fig. 5H). These results indicated that HMGCS1 may be involved in the functions of VIM-AS1 in prostate cancer cells.

VIM-AS1 specifically interacts with IGF2BP2 in prostate cancer cells. To investigate the regulatory mechanisms of VIM-AS1 in prostate cancer, the subcellular localization of VIM-AS1 was further explored. RT-qPCR analysis of the nuclear and cytoplasmic fractions (Fig. 6A) and FISH analysis (Fig. 6B) showed that VIM-AS1 was present in both the cytoplasm and the nucleus of C4-2 cells. RNA pull-down assays were performed to identify VIM-AS1-interacting proteins. Several bands were identified as potential binding proteins that could be pulled down by biotinylated VIM-AS1 transcripts (Fig. 6C). By searching the functions of 13 potential

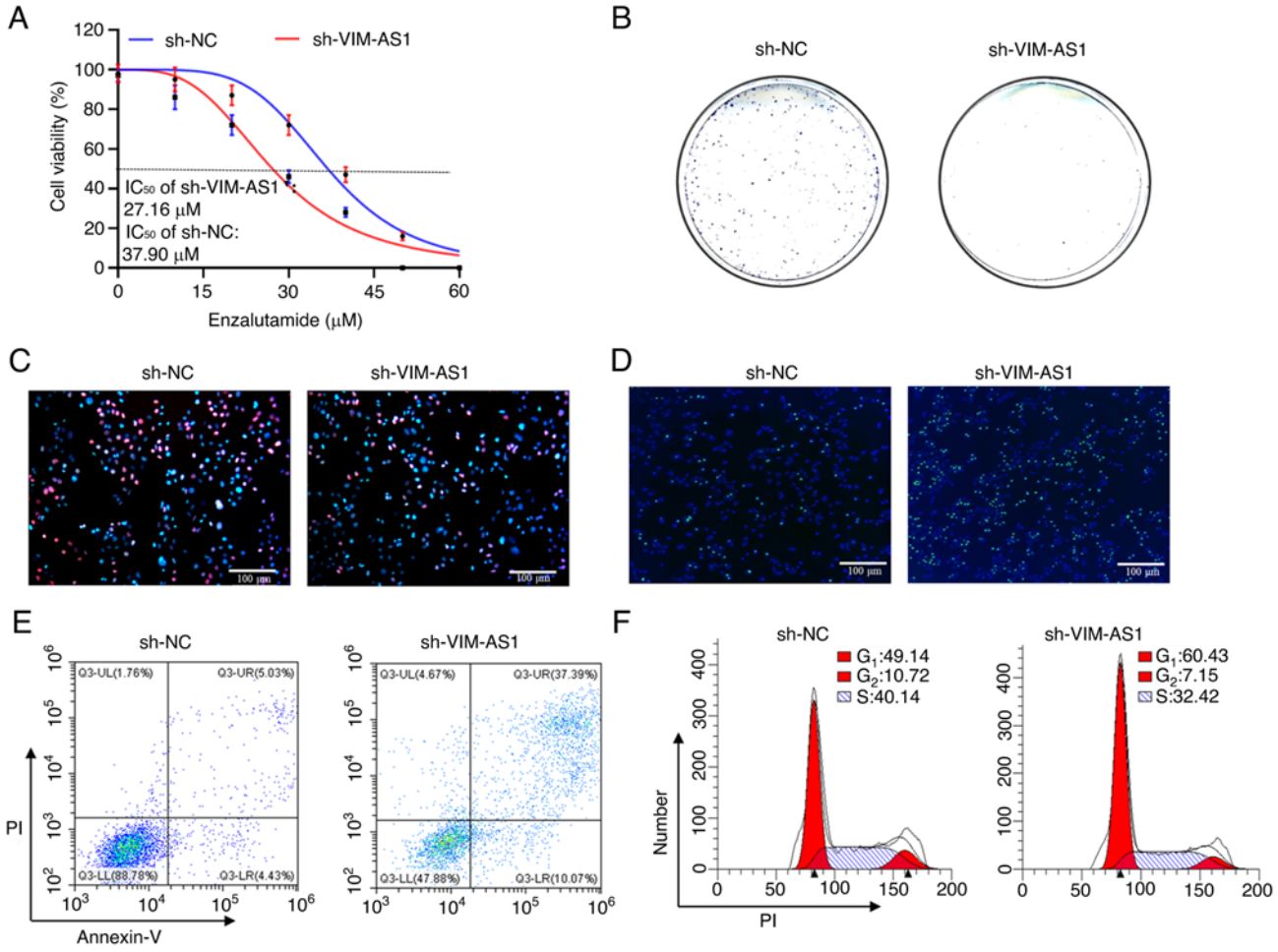

Figure 3. Effect of VIM-AS1 knockdown in C4-2 cells on enzalutamide sensitivity and cell proliferation. (A) Effect of VIM-AS1 knockdown on the viability of C4-2 cells treated with different concentrations of enzalutamide for 72 h as detected using a Cell Counting Kit-8 assay. (B) Effect of VIM-AS1 knockdown on the colony formation of C4-2 cells. (C) Effect of VIM-AS1 knockdown on the proliferation of C4-2 cells as detected using a 5-ethynyl-2'-deoxyuridine assay. Scale bar, 100 μm. (D) Effect of VIM-AS1 knockdown on the apoptosis of C4-2 cells as detected using a TUNEL assay. Scale bar, 100 μm. (E) Effect of VIM-AS1 knockdown on the apoptosis of C4-2 cells as detected using flow cytometry. (F) Effect of VIM-AS1 knockdown on the cell cycle distribution of C4-2 cells as detected using flow cytometry. sh-NC, normal scramble short hairpin RNA.

VIM-AS1 binding proteins in published studies, IGF2BP2, a major differential band precipitated in LNCaP lysates of RNA pulldown (Fig. 6D) and mass spectrometry (Fig. S3), was confirmed as the only steroid biosynthesis-related protein with a molecular mass of 25-116 kDa (32). RNA pull-down assays and western blotting further confirmed that VIM-AS1 interacted with IGF2BP2 in LNCaP and C4-2 cells (Fig. 6E). The enrichment of VIM-AS1 in the precipitates of the IGF2BP2 antibody but not IgG antibody were further confirmed by RIP assays (Fig. 6F). VIM-AS1 knockdown or overexpression exhibited no influence on IGF2BP2 mRNA and protein levels (Fig. 6G and H). In summary, these results indicated that VIM-AS1 directly bound to IGF2BP2 protein but did not regulate its expression in prostate cancer cells.

VIM-AS1/IGF2BP2 complex mediates the regulation of HMGCS1 mRNA stability. As IGF2BP2 is a known N^6-methyladenosine (m6A) reader and serves a pivotal role in downstream mRNA stabilization (33), it was next assessed whether IGF2BP2 was involved in the regulation of HMGCS1 expression. First, the HMGCS1 mRNA m6A modification status was predicted using Whistle (34). The results demonstrated that the 3'-untranslated region (3'-UTR) of HMGCS1 mRNA contained three m6A modification sites (Fig. S4). RT-qPCR and western blotting revealed that knockdown of IGF2BP2 or transfection with si-HMGCS1 inhibited VIM-AS1 overexpression vector transfection-induced HMGCS1 upregulation (Figs. 7A and B, and S5A and B). Overexpression of IGF2BP2 or HMGCS1 reversed sh-VIM-AS1-induced HMGCS1 downregulation (Figs. 7C and D, and S5C and D). mRNA stability assays demonstrated that overexpression of VIM-AS1 enhanced HMGCS1 mRNA stability, and enhancement of HMGCS1 mRNA stability was decreased following IGF2BP2 knockdown (Fig. 7E). Furthermore, knockdown of VIM-AS1 decreased HMGCS1 mRNA stability, and this was reversed by overexpression of IGF2BP2 (Fig. 7F). Collectively, these data suggested that the VIM-AS1/IGF2BP2 axis may exert roles in HMGCS1 post-transcriptional mRNA stabilization.

HMGCS1 is a functional mediator of VIM-AS1 in the regulation of proliferation and enzalutamide sensitivity in prostate cancer. To further elucidate the functional interplay between HMGCS1 and VIM-AS1 in the regulation of proliferation and enzalutamide sensitivity of prostate cancer, HMGCS1

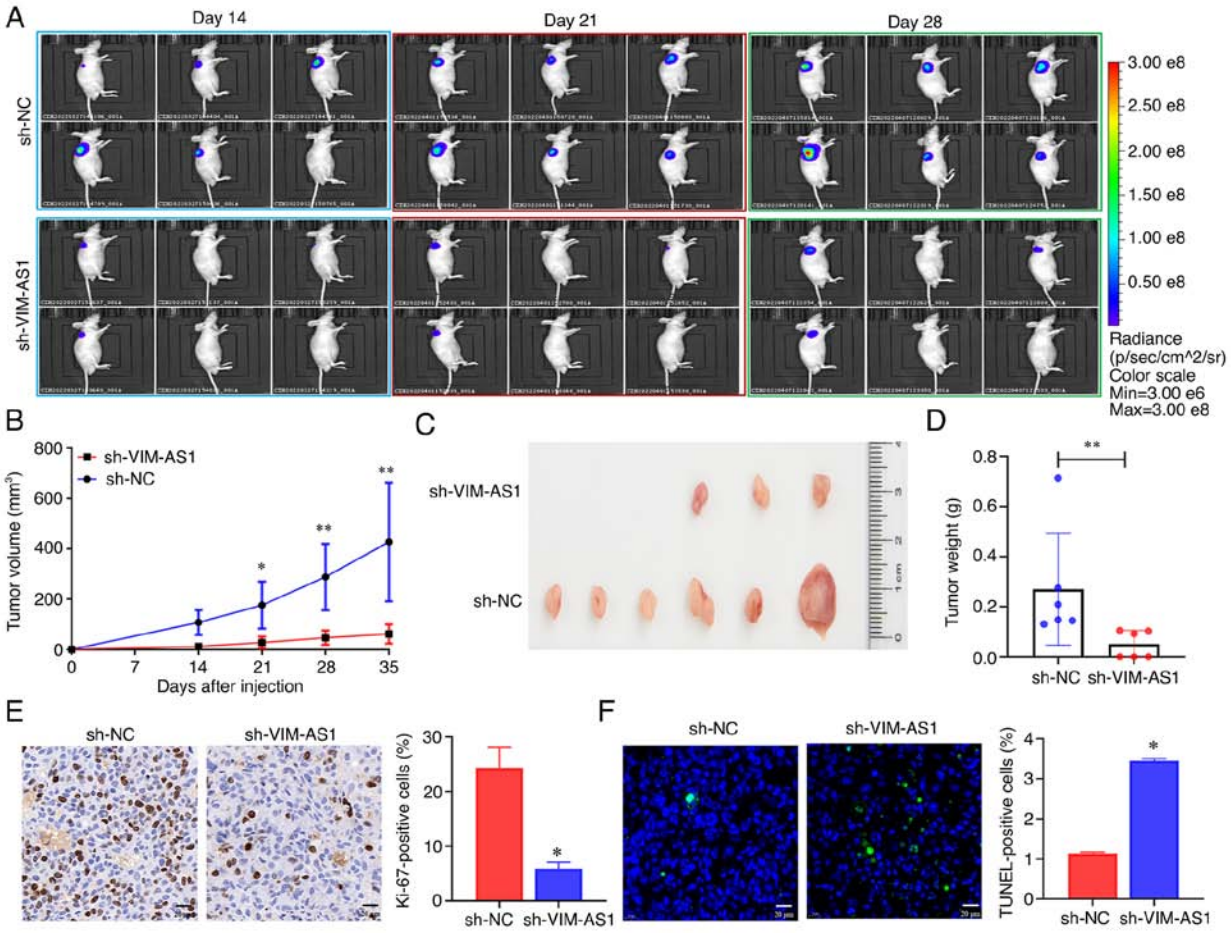

Figure 4. Effect of VIM-AS1 knockdown on tumor growth of C4-2 cells *in vivo*. (A) Effect of VIM-AS1 knockdown on tumor growth in nude mice subcutaneously injected with C4-2 cells as detected using small animal imaging. (B) Tumor growth curves from the nude mice subcutaneously injected with C4-2 cells infected with sh-VIM-AS1 or sh-NC. (C) Images of resected tumors, the diameters of which were measured using the vertical ruler, from the sh-NC and sh-VIM-AS1 groups at 35 days after injection. (D) Weights of the resected tumors from the sh-NC and sh-VIM-AS1 groups. (E) Effect of VIM-AS1 knockdown on the proliferation of C4-2 cells *in vivo*. Representative images of Ki-67 staining. Scale bar, 20 μm. (F) Effect of VIM-AS1 knockdown on the apoptosis of C4-2 cells *in vivo*, detected using TUNEL assays. Scale bar, 20 μm. Data are presented as the mean ± SD of three independent repeats. *P<0.05 and **P<0.01 vs. sh-NC or as indicated. sh-NC, normal scramble short hairpin RNA.

expression was knocked down in VIM-AS1-overexpressing LNCaP cells and HMGCS1 was overexpressed in the VIM-AS1 knockdown C4-2 cells. Functional experiments revealed that knockdown of HMGCS1 expression abrogated the increase in proliferation (Figs. 8B and C, and S5F and G) and cells at S stage (Figs. 8F and S5J), and decrease in enzalutamide sensitivity (Figs. 8A and S5E), apoptosis levels (Figs. 8E and S5I) and cells at G1 stage (Figs. 8F and S5J) induced by VIM-AS1 overexpression in LNCaP cells. Overexpression of HMGCS1 ameliorated the increase in enzalutamide sensitivity (Figs. 8A and S5E), apoptosis level (Figs. 8E and S5I) and cells at G1 stage (Figs. 8F and S5J), and reduced the increase in proliferation (Figs. 8B and C, and S5F and G) and cells at S stage (Figs. 8F and S5J) induced by VIM-AS1 knockdown in C4-2 cells. These results indicated that HMGCS1 mediated the VIM-AS1-induced increase in proliferation and enzalutamide resistance in prostate cancer cells.

Discussion

The development of high throughput sequencing technologies, together with the advances in computational pipelines, has led to an explosion in the discovery of disease-related lncRNAs. An increasing number of lncRNAs have been identified as crucial regulators of multiple diseases, including prostate cancer (9-11,35-37). For example, Zhang *et al* (35) found that lncRNA DSCAM-AS1 was upregulated in prostate cancer, and promoted cancer progression by forming a positive feedback loop with forkhead box A1. Wen *et al* (36) also reported that lncRNA NEAT1 expression was higher in patients with prostate cancer with bone metastases, and it induced cancer cell metastasis to the lungs and bones via m6A. A recent study demonstrated that lncRNA NXTAR was downregulated in prostate cancer, and restoration of NXTAR expression could suppress prostate cancer cell proliferation and abrogate enzalutamide-resistant prostate xenograft tumor growth (37). However, the expression patterns and roles of lncRNAs in the progression from HSPC to CRPC should be further elucidated.

In previous study, the first expression profile of dysregulated lncRNAs between cell models of HSPC and CRPC was mapped, and it was found that there were 134 dysregulated lncRNAs in C4-2 cells compared with LNCaP cells (14). In addition, the expression of the four most upregulated lncRNAs, including plncRNA-1, Linc00963, SNHG17 and

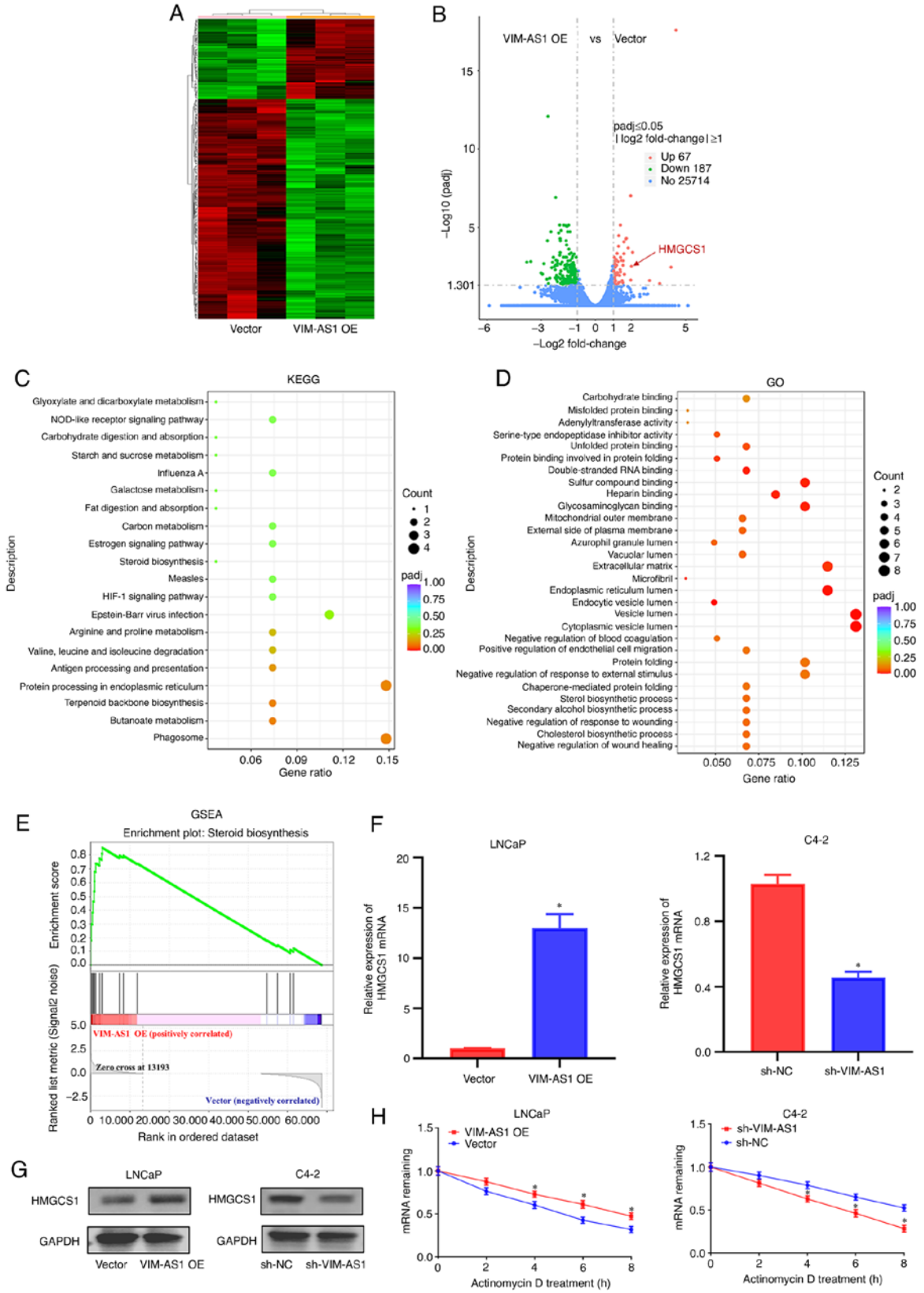

Figure 5. HMGCS1 is the downstream target of VIM-AS1 in prostate cancer cells. (A) Heat map analysis showing the upregulated and downregulated genes following VIM-AS1 overexpression in LNCaP cells. (B) Volcano plot showing the dysregulated genes (false discovery rate, >2; padj≤0.05) following VIM-AS1 overexpression in C4-2 cells. (C) KEGG pathway analysis showing the top 20 involved signaling pathways of the dysregulated genes following VIM-AS1 overexpression in C4-2 cells. (D) GO analysis showing the top 20 enriched biological processes of the dysregulated genes upon VIM-AS1 overexpression in C4-2 cells. (E) GSEA demonstrated that VIM-AS1 expression was significantly associated with 'Steroid biosynthesis'. (F) Effect of VIM-AS1 knockdown or overexpression on the mRNA expression levels of HMGCS1 in prostate cancer cells. (G) Effect of VIM-AS1 knockdown or overexpression on the protein expression levels of HMGCS1 in prostate cancer cells. (H) Effect of VIM-AS1 knockdown or overexpression on the stability of HMGCS1 mRNA in prostate cancer cells treated with actinomycin D for the indicated periods of time. Data are presented as the mean ± SD of three independent repeats. *P<0.05 vs. sh-NC or Vector. GO, Gene Ontology; GSEA, Gene Set Enrichment Analysis; HMGCS1, 3-hydroxy-3-methylglutaryl-CoA synthase 1; KEGG, Kyoto Encyclopedia of Genes and Genomes; sh-NC, normal scramble short hairpin RNA; padj, adjusted P-value.

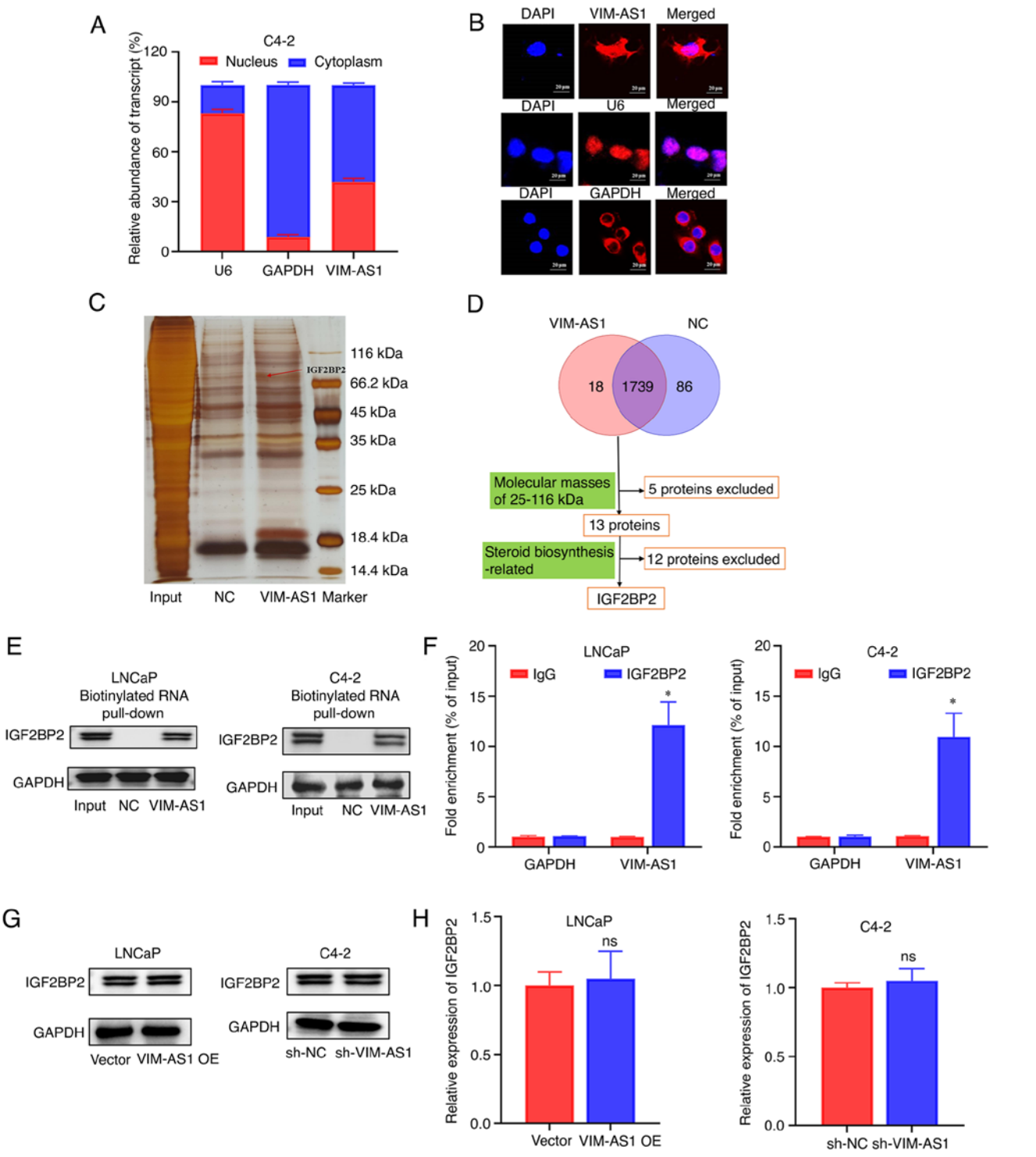

Figure 6. VIM-AS1 interacts with the RNA-binding protein IGF2BP2. (A) Relative VIM-AS1 levels in the nucleus and cytoplasm of C4-2 cells. GAPDH and U6 RNA were used as the loading controls for the cytoplasmic and nuclear fractions, respectively. (B) VIM-AS1 intracellular localization in C4-2 cells as detected by fluorescence *in situ* hybridization. GAPDH and U6 RNA served as positive controls for the cytoplasmic and nuclear fractions, respectively. Scale bar, 20 μm. (C) Potential binding proteins purified from RNA pull-down assays using a biotinylated VIM-AS1 probe or normal control probe. (D) Analysis flow chart for identification of steroid biosynthesis-related proteins that interact with VIM-AS1. (E) An interaction between VIM-AS1 and IGF2BP2 was identified using RNA pulldown and western blotting assays in LNCaP and C4-2 cells. (F) Enrichment of VIM-AS1 with IGF2BP2 antibody as detected by RNA immunoprecipitation. IgG was used as the control antibody. (G) Effect of VIM-AS1 knockdown or overexpression on the protein expression levels of IGF2BP2 in prostate cancer cells. (H) Effects of VIM-AS1 knockdown or overexpression on the mRNA expression levels of IGF2BP2 in prostate cancer cells. Data are presented as the mean ± SD of three independent repeats. *P<0.05 vs. IgG. IGF2BP2, insulin like growth factor 2 mRNA binding protein 2; NC, normal scrambled control probe; ns, not significant; sh-NC, normal scramble short hairpin RNA.

VIM-AS1, was validated in C4-2 cells (16). However, the study did not further explore the functions and mechanisms of the four lncRNAs in the progression of prostate cancer (16). Consistent with the findings of this study, a series of follow-up studies also revealed that these four lncRNAs were dysregulated and served pivotal roles in the development of prostate

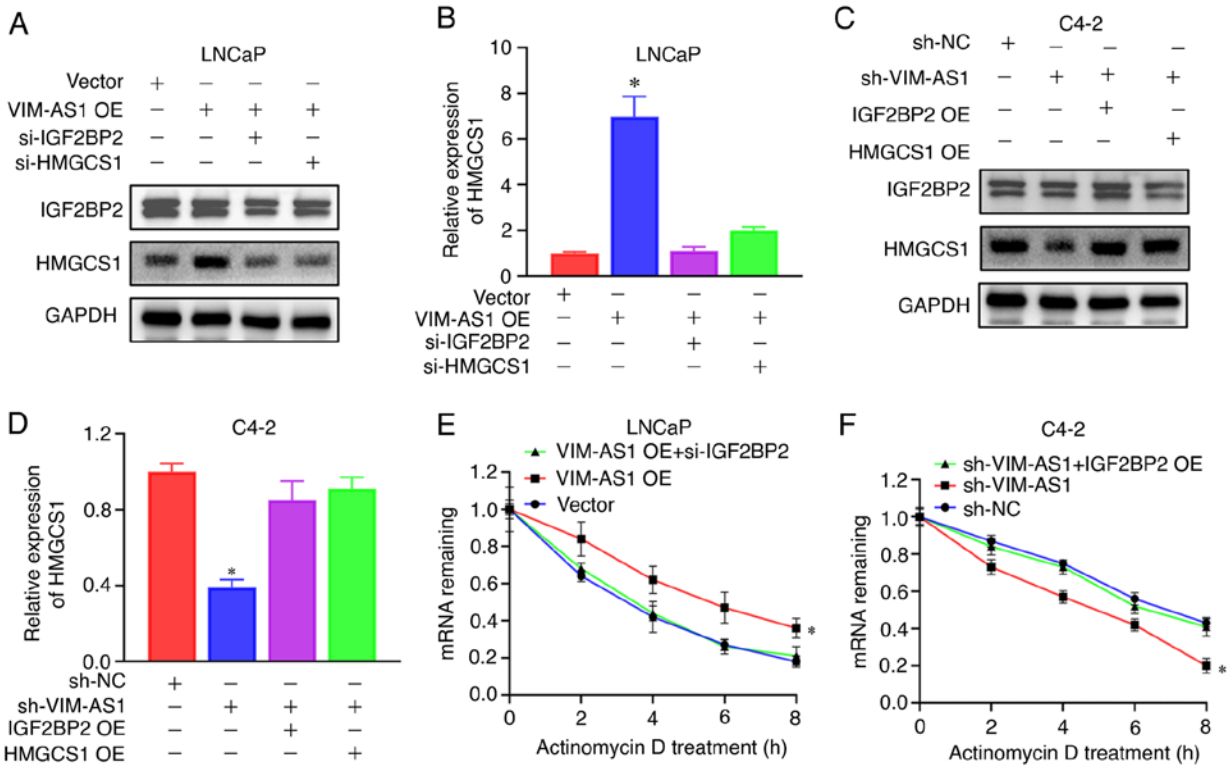

Figure 7. VIM-AS1 enhances HMGCS1 mRNA stability by binding with IGF2BP2. (A) Effect of VIM-AS1 overexpression and/or IGF2BP2/HMGCS1 knockdown on the protein expression levels of HMGCS1 in LNCaP cells. (B) Effect of VIM-AS1 overexpression and/or IGF2BP2/HMGCS1 knockdown on the mRNA expression levels of HMGCS1 in LNCaP cells. *P<0.05 (VIM-AS1 OE vs. Vector). (C) Effect of VIM-AS1 knockdown and/or IGF2BP2/HMGCS1 overexpression on the protein expression levels of HMGCS1 in C4-2 cells. (D) Effect of VIM-AS1 knockdown and/or IGF2BP2/HMGCS1 overexpression on the mRNA expression levels of HMGCS1 in C4-2 cells. *P<0.05 (sh-VIM-AS1 vs. sh-NC). (E) Effect of VIM-AS1 overexpression and IGF2BP2 knockdown on the mRNA stability of HMGCS1in LNCaP cells treated with actinomycin D for different lengths of time. *P<0.05 (VIM-AS1 OE vs. Vector). (F) Effect of VIM-AS1 knockdown and IGF2BP2 overexpression on the mRNA stability of HMGCS1 in C4-2 cells treated with actinomycin D for the indicated periods of time. *P<0.05 (sh-VIM-AS1 vs. sh-NC). Data are presented as the mean ± SD of three independent repeats. HMGCS1, 3-hydroxy-3-methylglutaryl-CoA synthase 1; IGF2BP2, insulin like growth factor 2 mRNA binding protein 2; NC, negative control; sh, short hairpin RNA; si, small interfering RNA.

cancer (17,19,38-42). Linc00963 has been reported to promote prostate cancer progression by modulating miR-655/tripartite motif containing 24 and the miR-542-3p/NOP2 nucleolar protein axes (17,38). SNHG17 has been demonstrated to enhance the acquisition of malignant phenotypes in prostate cancer cells by activating the β-catenin signaling pathway (39) or by targeting miR-144/CD51 (40). plncRNA-1 has been demonstrated to accelerate the progression of prostate cancer by inducing EMT (41) or by modulating the PTEN/AKT signaling pathway (42). Zhang *et al* (19) reported that VIM-AS1 expression was upregulated in prostate cancer tissues and promoted the proliferation and invasion of CRPC PC-3 cells by regulating EMT. Consistent with previous literature (17,19,38-42), our previous study also revealed that the knockdown of VIM-AS1 inhibited proliferation and restored the sensitivity to bicalutamide in CRPC C4-2 cells (43). However, the underlying mechanism by which VIM-AS1 modulates the development of prostate cancer has not yet been elucidated.

The current study further demonstrated that VIM-AS1 expression was upregulated in tumor tissues from patients with CRPC compared with patients with HSPC, which further indicated that VIM-AS1 may be involved in the progression from HSPC to CRPC. Subsequently, the effects of VIM-AS1 on proliferation and enzalutamide sensitivity were assessed using gain-and-loss functional experiments. VIM-AS1 markedly promoted cell proliferation and induced enzalutamide resistance *in vitro*. These findings were consistent with the expression patterns of VIM-AS1 in HSPC and CRPC tissues, and further indicated that VIM-AS1 acted as a pivotal regulator of tumor growth and sensitivity to anti-androgen therapy during the progression from HPSC to CRPC, and may thus be considered a potential therapeutic target for management of CRPC.

To elucidate the underlying mechanism by which VIM-AS1 regulated proliferation and enzalutamide sensitivity in prostate cancer cells, RNA-seq analysis was performed. HMGCS1 was found to be a potential downstream target and functional mediator of VIM-AS1 as it was one of the most upregulated genes in VIM-AS1-overexpressing LNCaP cells. Additionally, rescue assays indicated that upregulation of HMGCS1 reversed the effects of VIM-AS1 knockdown on the proliferation and enzalutamide sensitivity of prostate cancer cells. Previous studies have demonstrated that the mevalonate pathway was frequently dysregulated and involved in the carcinogenesis and progression of several types of cancer by modulating inflammation, cell proliferation and steroidogenesis (44,45). Consistently, HMGCS1, an established regulatory node in the mevalonate pathway, has also been found to be highly expressed in several types of cancer (30) and serves an important role in regulating cancer progression by mediating

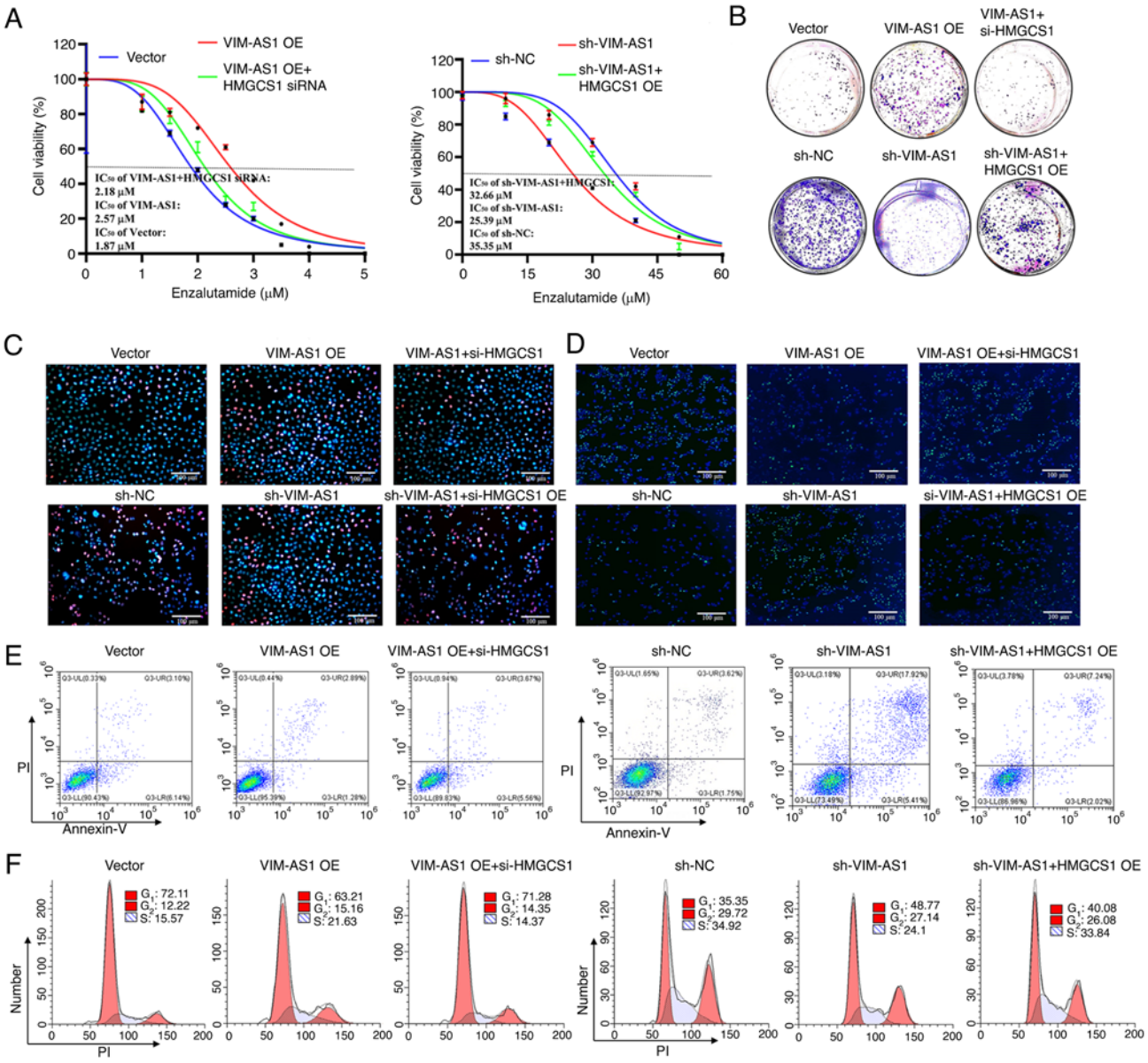

Figure 8. HMGCS1 is the functional mediator of VIM-AS1-induced proliferation acceleration and increased enzalutamide resistance in prostate cancer cells. (A) Effect of HMGCS1 knockdown or overexpression on the enzalutamide sensitivity of prostate cancer cells following VIM-AS1 overexpression or knockdown as detected using a Cell Counting Kit-8 assay. (B) Effect of HMGCS1 knockdown or overexpression on the colony formation of prostate cancer cells following VIM-AS1 overexpression or knockdown as detected using a colony formation assay. (C) Effect of HMGCS1 knockdown or overexpression on the proliferation of prostate cancer cells following VIM-AS1 overexpression or knockdown as detected using a 5-ethynyl-2'-deoxyuridine assay. Scale bar, 100 μm. (D) Effect of HMGCS1 knockdown or overexpression on the apoptosis of prostate cancer cells following VIM-AS1 overexpression or knockdown as detected using a TUNEL assay. Scale bar, 100 μm. (E) Effect of HMGCS1 knockdown or overexpression on the apoptosis of prostate cancer cells with VIM-AS1 overexpression or knockdown as detected using flow cytometry. (F) Effect of HMGCS1 knockdown or overexpression on the cell cycle distribution of prostate cancer cells following VIM-AS1 overexpression or knockdown as detected using flow cytometry. HMGCS1, 3-hydroxy-3-methylglutaryl-CoA synthase 1; sh-NC, normal scramble short hairpin RNA; si/siRNA, small interfering RNA.

cholesterol biosynthesis, including in gastric cancer (46), colorectal cancer (47) and breast cancer (48). Notably, a previous study indicated HMGCS1 was upregulated in CRPC PC-3 and 22Rv1 cells compared with HSPC LNCaP cells, and knockdown of HMGCS1 in 22Rv1 cells resulted in a reduction in cell viability and colony formation (49). In addition, Cheng *et al* (50) reported that HMGCS1 was associated with poor overall survival, and genetic variants of HMGCS1 were shown to act as protective factors for prostate cancer. Although several studies have highlighted HMGCS1 as a potential mediator of the progression of prostate cancer (49,50), to the best of our knowledge, the regulatory mechanism by which HMGCS1 exerts its effects on prostate cancer is largely unknown. The results of the present study not only further identified the important roles of HMGCS1 in the regulation of proliferation and enzalutamide sensitivity in prostate cancer cells but also found that VIM-AS1 was the potential upstream regulator of HMGCS1 in prostate cancer cells.

Mechanistically, the functional pattern of lncRNAs depends on their subcellular location. If lncRNAs are distributed primarily in the cytoplasm, they are likely to enhance target gene expression at the post-transcriptional level by binding

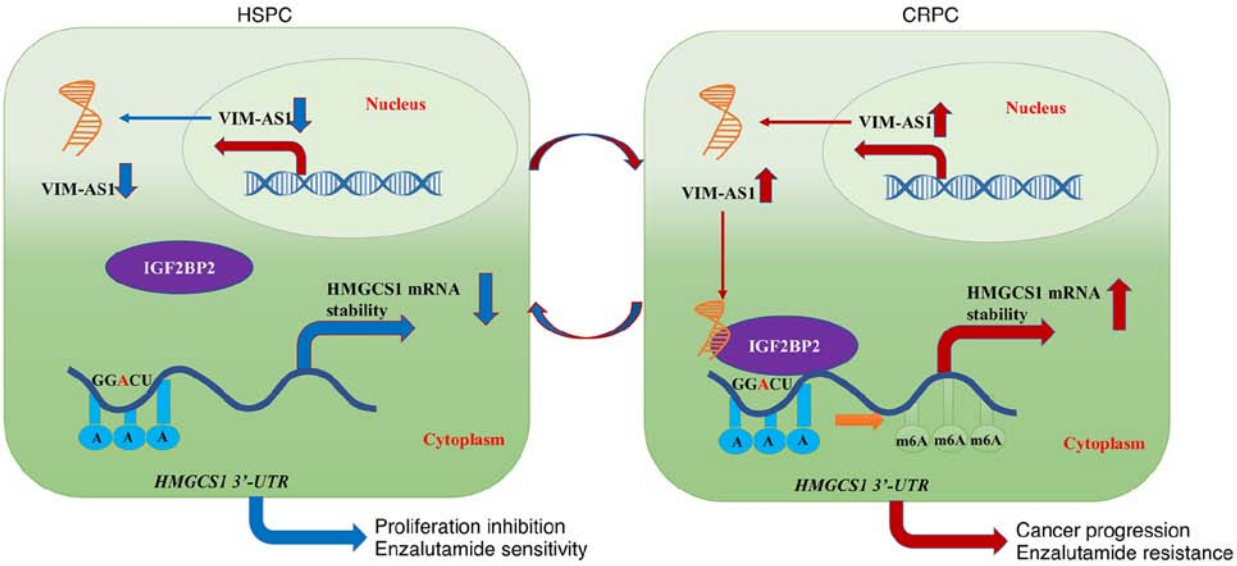

Figure 9. Graphical illustration of the mechanism by which the VIM-AS1/IGF2BP2/HMGCS1 axis enhances proliferation, increases enzalutamide resistance and promotes the progression from HSPC to CRPC. 3'-UTR, 3'-untranslated region; CRPC, castration-resistant prostate cancer; HMGCS1, 3-hydroxy-3-methylglutaryl-CoA synthase 1; HSPC, hormone-sensitive prostate cancer; IGF2BP2, insulin like growth factor 2 mRNA binding protein 2; m6A, N^6-methyladenosine.

with miRNAs or directly enhancing mRNA stability (51,52). For example, LINC00680, which is primarily located in the cytoplasm, promotes esophageal squamous cell carcinoma progression by functioning as a competing endogenous RNA to bind with miR-423-5p (51). Furthermore, Lang *et al* (52) found that lncRNA PCAT6, which is evenly distributed between the cytoplasm and nucleus, enhanced IGF1R mRNA stabilization by biding with the IGF2BP2 protein. However, if lncRNAs are primarily localized to the nucleus, they typically bind with proteins to regulate target gene expression at the transcriptional levels (53). For example, Chen *et al* (53) reported that lncRNA LBCS, which is primarily located in the nucleus suppressed SOX2 transcription by binding with heterogeneous nuclear ribonucleoprotein K and enhancer of zeste 2 polycomb repressive complex 2 subunit to mediate H3K27 tri-methylation. In the present study, it was revealed that VIM-AS1 was located in both the cytoplasm and the nucleus of prostate cancer cells and could directly interact with the IGF2BP2 protein. Previous studies have demonstrated that IGF2BP2 was both an important RNA-binding protein and an m6A reader (54,55). Numerous studies have indicated that IGF2BP2 could enhance mRNA stability by recognizing m6A modification sites (56,57). In the present study, it was shown that the 3'-UTR of HMGCS1 has three potential m6A modification sites. Furthermore, the present study revealed that the knockdown of IGF2BP2 abrogated the effects of VIM-AS1 on the mRNA stability of HMGCS1. Therefore, the results of the present study combined with those of previous studies (55-58) further elucidated the pivotal roles of IGF2BP2 in the regulation of HMGCS1 expression in prostate cancer.

In conclusion, it was demonstrated that VIM-AS1 was upregulated in patients with CRPC compared with patients with HSPC, and its upregulation induced enzalutamide resistance, promoted cell proliferation, and inhibited cell apoptosis in prostate cancer cells Furthermore, HMGCS1 was revealed to be the downstream target and functional mediator of VIM-AS1 in prostate cancer cells. Finally, it was also demonstrated that VIM-AS1 enhanced HMGCS1 mRNA stability and accelerated the progression of prostate cancer by binding with the IGF2BP2 protein (Fig. 9). Therefore, the present study contributed to the understanding of the regulatory mechanism by which VIM-AS1 and HMGCS1 exert their effects on prostate cancer and may provide novel biomarkers for the prediction of enzalutamide sensitivity.

Acknowledgements

Not applicable.

Funding

This work was supported by the Nature Science Foundation of Shaanxi Province (grant no. 2022JQ-774), China Postdoctoral Science Foundation funded project (grant no. 2021MD703953) and Fundamental Research Funds for the Central Universities (grant no. xzy012021077).

Availability of data and materials

The high-throughput sequencing datasets generated and/or analyzed during the current study are available in the GEO database repository (https://www.ncbi.nlm.nih.gov/geo/query/acc.cgi?acc=GSE220250). The other datasets used and/or analyzed during the current study are available from the corresponding author on reasonable request.

Authors' contributions

SJS, DHH, JLZ and YL performed the functional and animal experiments. DHH, JLZ and YL performed the RNA pulldown and RIP experiments. SJS and RZ confirm the authenticity of all the raw data. AGY and RZ designed the research study.

SJS, DHH and JLZ assembled the figures. SJS analyzed the data. SJS wrote the paper. All authors read and approved the final manuscript.

Ethics approval and consent to participate

All animal experiments complied with ethical regulations and were approved by the Animal Care and Use Committee of the Air Force Medical University (approval no. 20220967; Xi'an, China)

Patient consent for publication

Not applicable.

Competing interests

The authors declare that they have no competing interests.

References

1. Siegel RL, Miller KD, Fuchs HE and Jemal A: Cancer statistics, 2022. CA Cancer J Clin 72: 7-33, 2022.
2. Xia C, Dong X, Li H, Cao M, Sun D, He S, Yang F, Yan X, Zhang S, Li N and Chen W: Cancer statistics in China and United States, 2022: Profiles, trends, and determinants. Chin Med J (Engl) 135: 584-590, 2022.
3. Desai K, McManus JM and Sharifi N: Hormonal therapy for prostate cancer. Endocr Rev 42: 354-373, 2021.
4. Teo MY, Rathkopf DE and Kantoff P: Treatment of advanced prostate cancer. Annu Rev Med 70: 479-499, 2019.
5. Lin SR, Mokgautsi N and Liu YN: Ras and Wnt interaction contribute in prostate cancer bone metastasis. Molecules 25: 2380, 2020.
6. Tan YT, Lin JF, Li T, Li JJ, Xu RH and Ju HQ: LncRNA-mediated posttranslational modifications and reprogramming of energy metabolism in cancer. Cancer Commun (Lond) 41: 109-120, 2021.
7. Li S, Xie X, Peng F, Du J and Peng C: Regulation of temozolomide resistance via lncRNAs: Clinical and biological properties of lncRNAs in gliomas (Review). Int J Oncol 61: 101, 2022.
8. Yang G, Wu Y, Wan R, Sang H, Liu H and Huang W: The role of noncoding RNAs in the regulation, diagnosis, prognosis and treatment of osteosarcoma (Review). Int J Oncol 59: 69, 2021.
9. Lv Y, Wang Z, Zhao K, Zhang G, Huang S and Zhao Y: Role of noncoding RNAs in cholangiocarcinoma (Review). Int J Oncol 57: 7-20, 2020.
10. Sun X, Xin S, Zhang Y, Jin L, Liu X, Zhang J, Mei W, Zhang B, Ma W and Ye L: Long noncoding RNA CASC11 interacts with YBX1 to promote prostate cancer progression by suppressing the p53 pathway. Int J Oncol 61: 110, 2022.
11. Chen C, Tang X, Liu Y, Zhu J and Liu J: Induction/reversal of drug resistance in gastric cancer by non-coding RNAs (Review). Int J Oncol 54: 1511-1524, 2019.
12. Chen LJ, Wu L, Wang W, Zhai LL, Xiang F, Li WB and Tang ZG: Long non-coding 01614 hyperactivates WNT/β-catenin signaling to promote pancreatic cancer progression by suppressing GSK-3β. Int J Oncol 61: 116, 2022.
13. Zhang M, Wu L, Wang X and Chen J: LncKRT16P6 promotes tongue squamous cell carcinoma progression by sponging miR-3180 and regulating GATAD2A expression. Int J Oncol 61: 111, 2022.
14. Xie H, Zhao J, Wan J, Zhao J, Wang Q, Yang X, Yang W, Lin P and Yu X: Long noncoding RNA AC245100.4 promotes prostate cancer tumorigenesis via the microRNA1455p/RBBP5 axis. Oncol Rep 45: 619-629, 2021.
15. Huo W, Qi F and Wang K: Long noncoding RNA BCYRN1 promotes prostate cancer progression via elevation of HDAC11. Oncol Rep 44: 1233-1245, 2020.
16. Wang L, Han S, Jin G, Zhou X, Li M, Ying X, Wang L, Wu H and Zhu Q: Linc00963: A novel, long non-coding RNA involved in the transition of prostate cancer from androgen-dependence to androgen-independence. Int J Oncol 44: 2041-2049, 2014.
17. Bai M, He C, Shi S, Wang M, Ma J, Yang P, Dong Y, Mou X and Han S: Linc00963 promote cell proliferation and tumor growth in castration-resistant prostate cancer by modulating miR-655/TRIM24 axis. Front Oncol 11: 636965, 2021.
18. Hu CY, Wu KY, Lin TY and Chen CC: The crosstalk of long non-coding RNA and MicroRNA in castration-resistant and neuroendocrine prostate cancer: Their interaction and clinical importance. Int J Mol Sci 23: 392, 2021.
19. Zhang Y, Zhang J, Liang S, Lang G, Liu G, Liu P and Deng X: Long non-coding RNA VIM-AS1 promotes prostate cancer growth and invasion by regulating epithelial-mesenchymal transition. J BUON 24: 2090-2098, 2019.
20. Yin H, Zhang X, Yang P, Zhang X, Peng Y, Li D, Yu Y, Wang Y, Zhang J, Ding X, *et al*: RNA m6A methylation orchestrates cancer growth and metastasis via macrophage reprogramming. Nat Commun 12: 1394, 2021.
21. Sun J, Xiong Y, Jiang K, Xin B, Jiang T, Wei R, Zou Y, Tan H, Jiang T, Yang A, *et al*: Hypoxia-sensitive long noncoding RNA CASC15 promotes lung tumorigenesis by regulating the SOX4/beta-catenin axis. J Exp Clin Cancer Res 40: 12, 2021.
22. Livak KJ and Schmittgen TD: Analysis of relative gene expression data using real-time quantitative PCR and the 2(-Delta Delta C(T)) method. Methods 25: 402-408, 2001.
23. Feng T, Wei D, Zhao J, Li Q, Guo P, Yang X, Li M, Jiang Y and Luo Y: Construction of enzalutamide-resistant cell model of prostate cancer and preliminary screening of potential drug-resistant genes. Exp Bio Med (Maywood) 15: 1776-1787, 2021.
24. Chen S, Zhou Y, Chen Y and Gu J: fastp: An ultra-fast all-in-one FASTQ preprocessor. Bioinformatics 34: i884-i890, 2018.
25. Kim D, Langmead B and Salzberg SL: HISAT: A fast spliced aligner with low memory requirements. Nat Methods 12: 357-360, 2015.
26. Liao Y, Smyth GK and Shi W: featureCounts: An efficient general purpose program for assigning sequence reads to genomic features. Bioinformatics 30: 923-930, 2014.
27. Ashburner M, Ball CA, Blake JA, Botstein D, Butler H, Cherry JM, Davis AP, Dolinski K, Dwight SS, Eppig JT, *et al*: Gene ontology: Tool for the unification of biology. The gene ontology consortium. Nat Genet 25: 25-29, 2000.
28. The Gene Ontology Consortium: The gene ontology resource: 20 years and still GOing strong. Nucleic Acids Res 47: D330-D338, 2019.
29. Kanehisa M: Post-Genome Informatics. Oxford University Press, New York, NY, 2000.
30. Cai C, Wang H, He HH, Chen S, He L, Ma F, Mucci L, Wang Q, Fiore C, Sowalsky AG, *et al*: ERG induces androgen receptor-mediated regulation of SOX9 in prostate cancer. J Clin Invest 123: 1109-1122, 2013.
31. Zhou C, Wang Z, Cao Y and Zhao L: Pan-cancer analysis reveals the oncogenic role of 3-hydroxy-3-methylglutaryl-CoA synthase 1. Cancer Rep (Hoboken) 5: e1562, 2021.
32. Yang M, Gallo-Ebert C, Hayward M, Liu W, McDonough V and Nickels JT Jr: Human insulin growth factor 2 mRNA binding protein 2 increases MicroRNA 33a/b inhibition of liver ABCA1 expression and alters low-density apolipoprotein levels in mice. Mol Cell Biol 40: e00058-e00020, 2020.
33. Xu K, Dai X, Wu J and Wen K: N(6)-methyladenosine (m(6)A) reader IGF2BP2 stabilizes HK2 stability to accelerate the Warburg effect of oral squamous cell carcinoma progression. J Cancer Res Clin Oncol 148: 3375-3384, 2022.
34. Xu Q, Chen K and Meng J: WHISTLE: A functionally annotated high-accuracy map of human m(6)a epitranscriptome. Methods Mol Biol 2284: 519-529, 2021.
35. Zhang Y, Huang YX, Wang DL, Yang B, Yan HY, Lin LH, Li Y, Chen J, Xie LM, Huang YS, *et al*: LncRNA DSCAM-AS1 interacts with YBX1 to promote cancer progression by forming a positive feedback loop that activates FOXA1 transcription network. Theranostics 10: 10823-10837, 2020.
36. Wen S, Wei Y, Zen C, Xiong W, Niu Y and Zhao Y: Long non-coding RNA NEAT1 promotes bone metastasis of prostate cancer through N6-methyladenosine. Mol Cancer 19: 171, 2020.
37. Ghildiyal R, Sawant M, Renganathan A, Mahajan K, Kim EH, Luo J, Dang HX, Maher CA, Feng FY and Mahajan NP: Loss of long noncoding RNA NXTAR in prostate cancer augments androgen receptor expression and enzalutamide resistance. Cancer Res 82: 155-168, 2022.
38. Sun F, Wu K, Yao Z, Mu X, Zheng Z, Sun M, Wang Y, Liu Z and Zhu Y: Long noncoding RNA LINC00963 induces NOP2 expression by sponging tumor suppressor miR-542-3p to promote metastasis in prostate cancer. Aging (Albany NY) 12: 11500-11516, 2020.

39. Zhao H, Dong H, Wang P and Zhu H: Long non-coding RNA SNHG17 enhances the aggressiveness of C4-2 human prostate cancer cells in association with β-catenin signaling. Oncol Lett 21: 472, 2021.
40. Bai M, Lei Y, Wang M, Ma J, Yang P, Mou X, Dong Y and Han S: Long Non-coding RNA SNHG17 promotes cell proliferation and invasion in castration-resistant prostate cancer by targeting the miR-144/CD51 Axis. Front Genet 11: 274, 2020.
41. Jin Y, Cui Z, Li X, Jin X and Peng J: Upregulation of long non-coding RNA PlncRNA-1 promotes proliferation and induces epithelial-mesenchymal transition in prostate cancer. Oncotarget 8: 26090-26099, 2017.
42. Cui Z, Gao H, Yan N, Dai Y, Wang H, Wang M, Wang J, Zhang D, Sun P, Qi T, *et al:* LncRNA PlncRNA-1 accelerates the progression of prostate cancer by regulating PTEN/Akt axis. Aging (Albany NY) 13: 12113-12128, 2021.
43. Shi SJ, Zhang X, Han DH, Yang F, LI Y and Wang LJ: Long non-coding RNA VIM-AS1 promote proliferation and invasion of castrition-resistant prostate cancer C4-2 cells. Chin J Cell Mol Imm 36: 1083-1088, 2020.
44. Gobel A, Riffel RM, Hofbauer LC and Rachner TD: The mevalonate pathway in breast cancer biology. Cancer Lett 542: 215761, 2022.
45. Laka K, Makgoo L and Mbita Z: Cholesterol-lowering phytochemicals: Targeting the mevalonate pathway for anticancer interventions. Front Genet 13: 841639, 2022.
46. Wang IH, Huang TT, Chen JL, Chu LW, Ping YH, Hsu KW, Huang KH, Fang WL, Lee HC, Chen CF, *et al*: Mevalonate pathway enzyme HMGCS1 contributes to gastric cancer progression. Cancers (Basel) 12: 1088, 2020.
47. Yao W, Jiao Y, Zhou Y and Luo X: KLF13 suppresses the proliferation and growth of colorectal cancer cells through transcriptionally inhibiting HMGCS1-mediated cholesterol biosynthesis. Cell Biosci 10: 76, 2020.
48. Walsh CA, Akrap N, Garre E, Magnusson Y, Harrison H, Andersson D, Jonasson E, Rafnsdottir S, Choudhry H, Buffa F, *et al*: The mevalonate precursor enzyme HMGCS1 is a novel marker and key mediator of cancer stem cell enrichment in luminal and basal models of breast cancer. PLoS One 15: e0236187, 2020.
49. Ashida S, Kawada C and Inoue K: Stromal regulation of prostate cancer cell growth by mevalonate pathway enzymes HMGCS1 and HMGCR. Oncol Lett 14: 6533-6542, 2017.
50. Cheng Y, Meng Y, Li S, Cao D, Ben S, Qin C, Hua L and Cheng G: Genetic variants in the cholesterol biosynthesis pathway genes and risk of prostate cancer. Gene 774: 145432, 2021.
51. Xue ST, Zheng B, Cao SQ, Ding JC, Hu GS, Liu W and Chen C: Long non-coding RNA LINC00680 functions as a ceRNA to promote esophageal squamous cell carcinoma progression through the miR-423-5p/PAK6 axis. Mol Cancer 21: 69, 2022.
52. Lang C, Yin C, Lin K, Li Y, Yang Q, Wu Z, Du H, Ren D, Dai Y and Peng X: m(6) A modification of lncRNA PCAT6 promotes bone metastasis in prostate cancer through IGF2BP2-mediated IGF1R mRNA stabilization. Clin Transl Med 11: e426, 2021.
53. Chen X, Xie R, Gu P, Huang M, Han J, Dong W, Xie W, Wang B, He W, Zhong G, *et al:* Long noncoding RNA LBCS inhibits self-renewal and chemoresistance of bladder cancer stem cells through epigenetic silencing of SOX2. Clin Cancer Res 25: 1389-1403, 2019.
54. Li S, Wu Q, Liu J and Zhong Y: Identification of Two m6A Readers YTHDF1 and IGF2BP2 as immune biomarkers in head and neck squamous cell carcinoma. Front Genet 13: 903634, 2022.
55. Zhang Z, Xing Y, Gao W, Yang L, Shi J, Song W and Li T: N(6)-methyladenosine (m(6)A) reader IGF2BP2 promotes gastric cancer progression via targeting SIRT1. Bioengineered 13: 11541-11550, 2022.
56. Yao B, Zhang Q, Yang Z, An F, Nie H, Wang H, Yang C, Sun J, Chen K, Zhou J, *et al*: CircEZH2/miR-133b/IGF2BP2 aggravates colorectal cancer progression via enhancing the stability of m(6) A-modified CREB1 mRNA. Mol Cancer 21: 140, 2022.
57. Liu Y, Shi M, He X, Cao Y, Liu P, Li F, Zou S, Wen C, Zhan Q, Xu Z, *et al*: LncRNA-PACERR induces pro-tumour macrophages via interacting with miR-671-3p and m6A-reader IGF2BP2 in pancreatic ductal adenocarcinoma. J Hematol Oncol 15: 52, 2022.
58. Han L, Lei G, Chen Z, Zhang Y, Huang C and Chen W: IGF2BP2 regulates MALAT1 by serving as an N6-methyladenosine reader to promote NSCLC proliferation. Front Mol Biosci 8: 780089, 2021.